Journal Pre-proofs

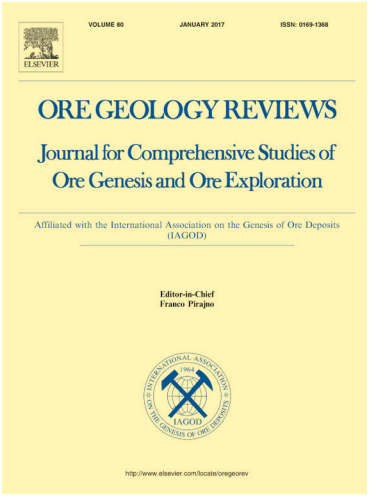


# Orogenic Au deposits with atypical metal association (Cu, Co, Ni): insights from the Pohjanmaa Belt, western Finland

Simon Hector, Clifford G. C. Patten, Jochen Kolb, Andressa de Araujo Silva, Benjamin F. Walter, Ferenc Molnár

PII: S0169-1368(23)00041-0
DOI: https://doi.org/10.1016/j.oregeorev.2023.105326
Reference: OREGEO 105326

To appear in: *Ore Geology Reviews*

Received Date: 20 October 2022
Revised Date: 13 January 2023
Accepted Date: 27 January 2023

Please cite this article as: S. Hector, C. G. C. Patten, J. Kolb, A. de Araujo Silva, B.F. Walter, F. Molnár, Orogenic Au deposits with atypical metal association (Cu, Co, Ni): insights from the Pohjanmaa Belt, western Finland, *Ore Geology Reviews* (2023), doi: https://doi.org/10.1016/j.oregeorev.2023.105326

# Orogenic Au deposits with atypical metal association (Cu, Co, Ni): insights from the Pohjanmaa Belt, western Finland.

Simon Hector[1, 2 +], Clifford G. C. Patten[1, 2], Jochen Kolb[1, 2],Andressa de Araujo Silva[1, 2], Benjamin F. Walter[1, 2] Ferenc Molnár[3, 4]

[1] Institute of Applied Geosciences, Chair of Geochemistry and Economic Geology, Karlsruhe Institute of Technology, 76131 Karlsruhe, Germany

[2] Laboratory for Environmental and Raw Materials Analysis (LERA), Adenauerring 20b, 76131 Karlsruhe, Germany

[3] Geological Survey of Finland, Vuorimiehentie 5, 02151 Espoo, Finland

[4] Department of Mineralogy, Institute of Geography and Geology, Eötvös Loránd University, 1177 Budapest, Pázmány Péter s. 1/C, Hungary

+corresponding author: simon.hector@kit.edu

*ORCID:* Simon Hector 0000-0002-8996-2251; Clifford Patten 0000-0001-8069-7271; Jochen Kolb 0000-0002-5633-1744; Andressa de Araujo Silva 0000-0002-5339-8409 ; Ferenc Molnár 0000-0002-1873-1915 ; Benjamin Florian Walter 0000-0003-2450-7722

Keywords: orogenic gold, Pohjanmaa Belt, cobalt, atypical metal association, Finland

## 1 ABSTRACT

The Laivakangas Au-Cu metallogenic area is characterised by orogenic Au deposits with both Au-only and with atypical (Au ± Cu, Co, Ni) metal associations. Here we study and compare four examples to better constrain the parameters controlling enrichment in base metals in addition to Au. We selected two typical Au-only deposits, the Laivakangas and the Huhta deposits and two orogenic Au deposits with atypical metal association, the Jouhineva Au-Cu-Co-Ag and the Kurula Au-Co deposits. All four deposits record multiple successive mineralisation events with local variations in their respective metal association. Two auriferous mineralisation events are identified, (1) a ubiquitous As-Au-(Co, Ni) event close to peak metamorphism (620-430°C) where Au occurs either as invisible Au in arsenides or as inclusion in arsenopyrite; (2) a later Cu(-Au)-rich sulfide event on the retrograde path where Au locally occurs as free, native grains along with chalcopyrite. From S isotope studies of the sulfide and sulfarsenide minerals and relations

between the deposits and surrounding rocks, we propose that the variation in metal association of the ore fluid is linked to the diversity of lithologies involved in metamorphic fluid production. Multi-event hydrothermal mineralisation and relatively reduced redox conditions appear critical to increase the Au endowment in a deposit and to introduce atypical metals. Results of this study provide a new comprehension of the variability of metal association in orogenic Au deposits of the Laivakangas Au-Cu metallogenic area and elsewhere.



# 2 INTRODUCTION

Precambrian orogenic Au deposits are epigenetic, and commonly hosted in greenstone belts. They usually form at post-peak metamorphic conditions in an active orogenic setting, along transcrustal faults under transpressive or compressive stress, and within a broad PT window (150-700°C; 0.5-7kbar) (Gebre-Mariam et al. 1995; Goldfarb et al. 2001, 2005; Groves et al. 1998; Kolb et al. 2015). Orogenic Au deposits, also known as Au-only deposits, usually contain only Au as a commodity (Eilu 2015; Goldfarb and Groves 2015; Groves et al. 1998). Some deposits, however, known as orogenic Au deposits with atypical metal association, show economic enrichment in Co, Ni and/or Cu, which can be exploited as by-products (Eilu 2015). These deposits are present in several orogenic Au districts worldwide such as in northern Finland (e.g. Central Lapland Greenstone Belt, Kuusamo Belt, Peräpohja Belt; Eilu 2015), northern Australia (Pine Creek), South Africa (Pilgrim's Rest) and in Mali (Loulo district) (Goldfarb and Groves 2015; Lawrence et al. 2013). This sub-type of orogenic Au deposits, although scarce, shows interesting economic value due to the polymetallic nature of the deposits. However, formation, and more specifically, processes leading to enrichment in base metals in relation to Au remain poorly understood.

The Paleoproterozoic orogenic belts of Finland and their related orogenic Au deposits with typical and atypical metal associations have been extensively studied; e.g. Central Lapland Greenstone Belt, Kuusamo Belt, Peräpohja Belt and to a lesser extent, the Pohjanmaa Belt (Fig. 1-A - Molnár et al. 2018; Pankka and Vanhanen 1992; Vanhanen et al. 2015; Vasilopoulos et al. 2021). These types of orogenic Au deposits share many similar features. They occur together in greenstone and schist belts along the same shear zones, they form over extended periods in multi-event hydrothermal systems during the same geodynamic event and display overall similar type of ore (Kurhila et al. 2017; Molnár et al. 2017; Vanhanen 2001; Vasilopoulos et al. 2021, 2022; Witt et al. 2020). Orogenic Au deposits with atypical metal association show distinctive endowments; the ones from the Central Lapland Greenstone and Pohjanmaa belts are enriched in Au-Cu ± (Ag, Co, Ni) and those from the Kuusamo and Peräpohja belts are rich in Au-Co ± (Cu, U, LREE) (Eilu 2015). Coexistence of orogenic Au deposits with typical and atypical metal associations along the same structures

raises questions regarding the source of the metals, nature of the fluids and relative timing of formation of the different ore types. Several mechanisms have been proposed to account for the diverse base metal association in atypical orogenic Au deposits. Goldfarb et al. (2001) highlight that orogenic Au deposits with high base metal content tend to occur in deformed Paleoproterozoic intracratonic basins. These basins can contain evaporitic rocks and salt-rich brines which can generate saline metamorphic fluids, promoting base metal mobilisation via chloride-complexes (Haverinen 2020; Qiu et al. 2021; Tapio et al. 2021; Vasilopoulos et al. 2021; Yardley 2005; Yardley and Graham 2002). Alternatively, orogenic Au deposits with atypical metal association can be spatially associated with intrusions; these are sometimes classified as porphyry Cu-Au deposits overprinted by orogenic Au mineralisation, in an attempt to account for their atypical metal association, even if the genetic link with the intrusion is not explicit (e.g. Jouhineva Au-Cu-Co-Ag deposit; Geological Survey of Finland 2019b; see also the Chibougamau Cu-Au(-Mo) mining district; Pilote et al. 1995). Finally, multi-event mineralisation is a common feature in orogenic Au deposits with atypical metal association, with different metals being enriched at different mineralisation events; highlighting the complexity of these deposits (Molnár et al. 2017; Novoselov et al. 2015; Patten et al. 2022; Vanhanen 2001; Vasilopoulos et al. 2022).

In this study, we investigate typical orogenic Au deposits (Laivakangas and Huhta) and orogenic Au deposits with atypical metal association (Jouhineva and Kurula) from the Pohjanmaa Belt, in western Finland, to better understand the mechanisms leading to different metal endowment in orogenic Au deposits. We highlight that orogenic Au mineralisation in the Pohjanmaa Belt is related to two main mineralisation events with different metal association. These events are expressed by various intensity in the different deposits and account for the observed metal enrichment in the deposits.

## 3 REGIONAL GEOLOGY OF THE POHJANMAA BELT

Finland lies within the Fennoscandian Shield. Its Precambrian geology incorporates the Archean cratons of Norbotten, Kola and Karelia in the north and east and by a Paleoproterozoic part, the Svecofennian domain, in the south and west. The main Archean domain is the Karelian province, where Archean rocks are partially covered by Paleoproterozoic rocks, forming greenstone belts with numerous orogenic Au deposits (Fig. 1-A) (e.g. Central Lapland Greenstone Belt, Peräpohja Belt, Kuusamo Belt - Eilu 2015; Hanski and Huhma 2005; Laajoki K. 2005). The contact between the Karelian province and the Svecofennian domain is marked by the Raahe-Ladoga Shear Zone. The Paleoproterozoic geology of Finland is the result of the complex Svecofennian orogeny, leading to the formation of the Fennoscandian shield. Recent models suggest the evolution of the diachronous Svecofennian orogeny comprised

five distinct, but temporally overlapping orogenic events, each of which dominated within specific spatially separated belts that were progressively amalgamated. They are: the Lapland-Kola orogeny (ca. 1960 to ca. 1870 Ma), the Lapland-Savo orogeny (ca. 1930 to ca. 1890 Ma), the Fennian orogeny (ca. 1900 to ca. 1850 Ma), the Svecobaltic orogeny (ca. 1840 to ca. 1780 Ma) and the Nordic orogeny (ca. 1820 to ca. 1770 Ma) (Korja et al. 2006; Lahtinen et al. 2005). The formation of the Fennoscandian shield started with the accretion of the Archean cratons of Kola, Karelia and Norbotten during the Lapland-Kola orogeny. In the south, accretion of the Keitele micro-continent and Paleoproterozoic volcano-sedimentary arcs against the Karelian Province during the Lapland-Savo orogeny and later orogenies led to the formation of the Svecofennian province and its volcano-sedimentary belts containing orogenic Au deposits (Savo Belt, Pohjanmaa Belt, Tampere Belt, Pirkanmaa Belt, Häme Belt and Uusimaa Belt). The oldest is the Savo Belt, thrust above the Karelian province during the Lapland-Savo orogeny (Korja et al. 2006; Lahtinen et al. 2005). The following Fennian orogeny led to the formation of the Pohjanmaa Belt. The Skellefte district in Sweden is proposed to be the continuation of the Pohjanmaa Belt (Lahtinen et al. 2014). The general crustal structure of the Svecofennian accretionary orogen is a north-east plunging succession of superposing nappes made of volcano-sedimentary units and granite intrusions of the Central Lapland Granitoid Complex (Mints et al. 2020).

The Pohjanmaa Belt corresponds now to the coast of Finland in the north-western part of the former Western Finland Province. This schist belt is limited to the north by the Raahe-Ladoga Shear Zone (Nironen et al. 2002), to the east by the Savo Belt and the Central Finland Granitoid Complex, and continues to the south-west as the Pirkanmaa and Tampere belts (Lahtinen et al. 2014) (Fig. 1-A). The Pohjanmaa Belt is divided into the Ylivieska and the Evijärvi fields, which are considered to represent a volcanic-arc and accretionary prism, respectively (Fig. 1-A) (Kähkönen 2005). Syn-kinematic and post-kinematic granites (e.g. Rautio batholith) belonging to the Central Lapland Granitoid Complex intruded the Pohjanmaa Belt (Haapala and Rämo, 2015; Luukas et al. 2017) (Fig. 1-A). The Ylivieska field is thrust south-westward over the Evijärvi field. The Evijärvi field is composed of various meta-sedimentary and mafic meta-volcanic rocks with mid-ocean-ridge basalt and within-plate basalt affinities (Fig. 1-A). They are considered part of the lower sedimentary group of the central part of the Svecofennian orogen (Lahtinen et al. 2002). Peak metamorphism in the Pohjanmaa Belt reached low- to medium-amphibolite facies at ca. 1890-1880 Ma in its central part, but increases to the south-west up to lower-granulite facies conditions where crustal melting led to the formation of the Vaasa Batholith (Chopin et al. 2020; Kähkönen 2005; Mäkitie 1999, 2000; Mäkitie et al. 2012; Mäkitie and Lahti 1991; Vaarma 1990; Vaarma and Pipping 1997). The Ylivieska field contains ca. 1900 to 1880 Ma arc-type meta-volcanic

and meta-sedimentary rocks belonging to the upper sedimentary group of Central Svecofennia (Kähkönen 2005) (Fig. 1-A). The meta-volcanic rocks are characteristic of a shallow water to sub-aerial environment and range from basalt to K-rhyolite with calc-alkaline, mature island-arc affinity (Kähkönen 2005). The meta-sedimentary rocks are typical of fluvial and shallow water environments (Lahtinen et al. 2002). The Ylivieska plutonic suite locally intruded the meta-volcano-sedimentary rocks. It consists mainly of syn-orogenic, mafic, layered intrusions with minor ultramafic rocks and local magmatic Ni-Cu-Co sulfide occurrences (Kiuttu 2020; Luukas et al. 2017) (Fig. 1-A). It formed at ca. 1880 Ma during the accretion stage of the Fennian Orogen along subvertical shear zones (Peltonen 2005).



### 3.1 Metallogeny of the Pohjanmaa Belt

The Au deposits of the Pohjanmaa Belt are mostly located in the Laivakangas Au-Cu metallogenic area within the Ylivieska field, where the main mineralisation style is orogenic Au with a few porphyry Cu-Au and porphyry Mo deposits (Fig. 1-A) (Eilu et al. 2012). The orogenic Au deposits locally contain anomalous Cu and/or Co and Ni (Eilu 2015; Isohanni 1984; Sipilä 1988). They are usually located close to shear zones and show spatial association with syn-orogenic, ca. 1890-1860 Ma tonalite and granodiorite (Gaál and Sundblad 1990; Nironen 2005). There is no precise age data of the Au deposits. Nevertheless, Sundblad et al. (1993) studied isotopic Pb data in galena from epigenetic Au deposits in the Skellefte District and the Pohjanmaa Belt, and suggest that the Au deposits formed approximately 10 to 20 m.y. after the surrounding host rocks, constraining their age of formation at approximately 1880-1850 Ma. The Laivakangas Au-Cu metallogenic area comprises the Hitura Ni-Co metallogenic area in its central part (Fig. 1-A) (Eilu et al. 2012). It contains mainly small magmatic Ni-Cu-Co sulfide deposits in syn-orogenic ultramafic to mafic layered intrusions (1890-1870 Ma; Peltonen 2005). The orogenic Au deposits with typical and atypical metal association share a similar geological setting (Fig. 1-B to D). All the deposits comprise sets of quartz veins and disseminated ore hosted in meta-volcanic to meta-sedimentary rocks and share similar metamorphic grade. However, the deposits display different metal associations and contents.

## 4 Orogenic Au deposits of the Pohjanmaa Belt

### 4.1 The Laivakangas and the Huhta Au deposits

The Laivakangas Au deposit is a mine located in the north of the Pohjanmaa Belt (Fig. 1-A). It is exploited in two open-pits and has 48.58 tonnes of Au reserve (Bektas and Vathavooran 2019). It is classified as a typical orogenic Au deposit, although it has metal zonation fromAu-As to Au-Cu and Au-Mo-W, interpreted to result from interaction

with magmatic fluids in the deposit formation (Geological Survey of Finland 2019d; Mäkelä 1984). The host rocks consist of a mafic meta-volcanic unit, intruded by granodiorite prior to regional metamorphism (Fig. 1-B). Mineralized sets of quartz veins cross-cut the host rocks. Younger syeno-granite and dolerite dykes post-date regional peak metamorphism and cross-cut all the previous lithologies and veins. The host rocks reached peak middle amphibolite facies conditions at 575 ± 50°C and 5 kbar (Mäkelä 1984) at ca. 1890-1860 Ma, according to regional metamorphic peak dating on monazite U-Pb data from migmatite (Hölttä et al. 2019). The ore is hosted in sheeted quartz-sulfide vein arrays in several subparallel shear zones hosted in meta-volcanic rocks and meta-granodiorite. Individual veins are planar, narrow (2-5 mm, rarely 2-5 cm wide) and display localized pinch and swell structures, although the auriferous structure is continuous over tens of metres (Bektas and Vathavooran 2019).

The Huhta Au deposit comprises a typical orogenic Au mineralisation. It is located in the central western part of the Ylivieska field, within the Laivakangas Au-Cu metallogenic area, and is in direct proximity to the Hitura Ni-Co metallogenic area (Fig. 1-A) (Geological Survey of Finland 2019a). There is no estimation of resources available for this deposit. The host rocks reached peak lower amphibolite facies conditions at 545 ± 30°C at 1810-1800 Ma (Hölttä et al. 2019; Hölttä and Heilimo 2017). The deposit is formed by two main lode zones hosted by intermediate to felsic meta-volcanic rocks (Fig. 1-C). The lodes are subvertical and are oriented west-northwest. The ore is located in quartz-sulfide veins and shear bands in the host rocks.

## 4.2 The Jouhineva Au-Cu-Co-Ag and the Kurula Au-Co deposits

The Jouhineva (also known as Pölla) deposit is located 2.8 kilometres north-west of the Huhta deposit (Fig. 1-C), along the same tectonic structure. It lies within the Laivakangas Au-Cu metallogenic area close to the Hitura Ni-Co metallogenic area (Fig. 1-A). Test mining of 5000 t of mineralisation from an open pit in 1984 produced 40.5 tonnes of Cu, 4.5 kilogrames of Au, 40 kilogrames of Ag and 9 tonnes of Co (Geological Survey of Finland 2019b). The host rocks are lower amphibolite facies meta-andesite and intermediate meta-tuff (Geological Survey of Finland 2019b). Metamorphic peak conditions reached temperatures of 545 ± 30°C at 1810-1800 Ma (Hölttä et al. 2019; Hölttä and Heilimo 2017). The mineralisation is hosted by quartz-sulphide veins and shear zones that are up to 6 m wide and 20-200 m long, forming a set of subparallel, near-vertical, north-west-trending lodes.

The Kurula Au-Co deposit lies in both the Laivakangas Au-Cu and Hitura Ni-Co metallogenic areas, located in the central part of the Pohjanmaa Belt (Fig. 1-A; D) and is classified as an atypical orogenic Au deposit (Geological

Survey of Finland 2019c). There is no estimation of resources available for this deposit. The host rocks reached the middle amphibolite facies at 620 ± 40°C between 1870-1800 Ma (Hölttä et al. 2019; Hölttä and Heilimo 2017). The deposit comprises a mineralized quartz-tourmaline-arsenide-sulfide vein network hosted in intermediate to felsic meta-volcanic rocks at the contact between meta-volcanic and meta-sedimentary units of the Ylivieska Group (Geological Survey of Finland 2019c; Sipilä 1983, 1988).



# 5 SAMPLING AND ANALYTICAL METHODS

Field work was carried out in the northern and southern pits of the Laivakangas mine where 14 representative samples of the different host and mineralized rocks were collected. In addition, 39 representative samples of mineralized veins and host rocks were collected from 10 drill cores at different depth intervals (ESM 1). Drill core sampling was performed at the drill core storage facility of the Geological Survey of Finland in Loppi where 75, 31 and 40 samples of the Jouhineva, Huhta and Kurula deposits have been collected respectively. Representative samples of mineralized veins and different wall and host rocks were collected from the drill cores at different depth intervals according to the petrological features and geochemical data provided by the GTK (ESM 1). The drill cores of the Jouhineva deposit showing the highest Co content are already oversampled and could not be resampled.

After careful investigation, 98 polished thin sections were prepared for petrological study. Petrography of ore and host rock was studied using transmitted and reflected light microscopy and scanning electron microscopy using a TESCAN VEGA 3 scanning electron microscope (SEM). Ore mineral composition was determined by electron microprobe analysis (EPMA) using a JEOL 8900 Superprobe at the Eberhard Karls University of Tübingen. The following elements were measured: Ag, Au, As, Bi, Co, Cu, Fe, Hg, Ni, S, Sb, Zn (ESM 2). Operating conditions were an accelerating voltage of 25 kV at a probe current of 20 nA with a focused beam. $K_\alpha$-lines were used for As, Co, Fe, Ni, S, Zn; $K_\beta$-lines for Cu; $L_\alpha$-lines for Au, Ag, Bi, Hg and Sb. X-ray lines and background positions were selected to minimize interference during analysis. Overlap correction was applied for Au and Zn. PhiRhoZet correction was applied for data reduction. Native metals were used as calibration standards for Ag, Au, Bi, Co, Cu, Ni and Zn, and pyrite for Fe and S, cinnabar for Hg, stibnite for Sb, and GaAs for As.

Sulfur isotope analysis was performed in the Laboratory of Environmental and Raw Materials Analysis (Institute of Applied Geosciences, Karlsruhe Institute of Technology) on monomineralic powders of sulfides (arsenopyrite, chalcopyrite, pyrite and pyrrhotite). The sulfides were carefully sampled with a micro-drill after

observation with a binocular microscope to control sample homogeneity. Each sulfide sample was divided into three portions containing 100 µg of S and packed with $V_2O_5$ as catalyst in tin cups. The samples were heated at 1020 °C and the combustion products were transported in a continuous He flow through a reactor to form $SO_2$. The resulting products were sorted by an Eurovector elemental analyser, ionized and analysed with an Isoprime isotopic ratio mass spectrometer (IRMS). Reference material data are provided in ESM 3.



# 6 RESULTS

## 6.1 GOLD-ONLY OROGENIC DEPOSITS

The Laivakangas, Huhta, Jouhineva and Kurula deposits formed in two hydrothermal events: (1) a ubiquitous As-Au (Co, Ni) event, locally subdivided in stages based on the mineralogy; (2) a Cu(-Au) sulfide event locally overprinting the previous event veins. A late barren alteration event affects the mineralized veins in the Laivakangas and Jouhineva deposits (Fig. 2).

### 6.1.1 Laivakangas Au deposit

The auriferous quartz veins of the Laivakangas deposit are typically millimetres to several centimetres wide and are generally parallel to the host rock foliation (Fig. 3-A, B). They cross-cut and overprint barren, feldspar-dominated hydrothermal veins (Fig. 3-D), and are mainly composed of quartz and K-feldspar with accessory chlorite, biotite, pumpellyite, titanite, ilmenite, rutile, apatite, scheelite, zircon and rare carbonates. They are mostly deformed showing undulose extinction of quartz. Two main mineralisation events are defined: (1) an As-Au(-Co) event forming auriferous quartz veins containing Ni-Co-Fe arsenide with invisible Au; (2) a sulfide (Cu-Au) event, locally overprinting the previous event, forming auriferous quartz-sulfide veins with free, native Au (Fig. 2-A; Fig. 4-A). Theevents are not ubiquitous, leading to different ore mineral populations and content within veins (Fig. 3-C to E).

During the mineralisation event 1, Ni-Co-Fe arsenides, mainly löllingite and minor clinosafflorite $(Co,Ni,Fe)As_2$), occur in the quartz veins as <1mm inclusions in younger arsenopyrite (Fig. 3-F to H). Löllingite is locally enriched in Co, Ni and Ag (Table 1, ESM 2). The vein selvedges show brown to black, centimetre-scale hydrothermal alteration halos with disseminated arsenopyrite and pyrite, and replacement of plagioclase by sericite and biotite by chlorite, in the first millimetres of the alteration halo.

The mineralisation event 2 is characterized by: a) new auriferous quartz veins which locally cross-cut the previous vein generation and contain pyrite (Py1), chalcopyrite, pyrrhotite and minor sphalerite, molybdenite, free grains of native Au and Bi-(Te, Au, Ag, Cu) minerals; and b) overprinting of the event 1 veins with replacement of the Ni-Co-Fe arsenides by arsenopyrite and formation of previously listed sulfides (Fig. 2-A). Arsenopyrite occurs as euhedral to subhedral grains which are locally fractured (Fig. 3-I). It is commonly zoned and/or has event 1 Ni-Co-Fe arsenide, Au and Bi-(Te, Au, Ag, Cu) inclusions (Fig. 3-F to I). It shows overall homogeneous composition with little to no Co and Ni (Table 1). Arsenopyrite grains containing an event 1 clinosafflorite or a Co-rich löllingite core have higher Co- and Ni-contents (up to 2.5 and 1.5 wt.%, respectively; Table 1, ESM 2). Arsenopyrite is also locally enriched in Ag, up to 330 ppm (Table 1). Chalcopyrite and pyrrhotite occur in the veins as grains parallel to the foliation or as fracture fills in the gangue minerals, mainly feldspar and quartz (Fig. 3-J and K). Chalcopyrite locally has cubanite exsolution lamellae (Fig. 3-J), and sphalerite and molybdenite inclusions. Pyrite (Py1) grains are commonly pristine in an assemblage with chalcopyrite and pyrrhotite. Visible Au is identified as native Au inclusions and as free, native Au grains among sulfides and in fractures of vein filling silicates. Gold inclusions represent 80 to 90 vol.% of the visible Au, and occur in arsenopyrite and Ni-Co-Fe arsenide and rarely, in pyrrhotite or chalcopyrite (Fig. 3-F to I). They commonly occur together with Bi-(Te, Au, Ag, Cu) minerals at a volumetric ratio of 1:5. Free, native Au grains represent 10 to 20 vol.% of the visible Au. They occur as <50µm grains in the gangue commonly along with Bi-(Te, Au, Ag, Cu) minerals and chalcopyrite in the auriferous quartz veins (Fig. 3-K). Bi-(Te, Au, Ag, Cu) minerals are found as tellurides and Bi-rich minerals, which tend to occur together in the following proportions: native Bi (30 vol.%), hedleyite (23 vol.%), pilsenite (16 vol.%), wittichenite (13 vol.%), bismite (10 vol.%), hessite (7 vol.%), volynskite (<2 vol.%) and maldonite (<2 vol.%). Gold grains can contain variable amounts of Ag (5.47-21.90 wt.%; Table 1, ESM 2). Pyrite (Py1) is either enriched in Cu (up to 8 wt.%) or in As (up to 6 wt.%) when altered and spatially related to chalcopyrite and arsenopyrite, respectively (Table 1, ESM 2). Pyrite is locally enriched in Ag, Bi, Co, Ni and Zn (Table 1). Chalcopyrite contains Ag and shows local enrichment in Au and Bi, up to 350 ppm and 4510 ppm, respectively (Table 1). Pyrrhotite contains traces of Cu, Ni and Ag (Table 1). This mineralisation event is associated with millimetre- to centimetre-scale, hydrothermal sericite-chlorite alteration haloes characterized by greenish-white-coloured zones. It shows partial to complete chloritisation of biotite and amphibole, sericitisation of plagioclase and K-feldspar and disseminated chalcopyrite, pyrrhotite and pyrite (Py1) in the hydrothermal alteration zone. Late chlorite-quartz veinlets locally cross-cut the host rock and earlier veins, forming additional pyrite, bornite and digenite (Fig. 2-A), which locally replace chalcopyrite (Fig. 3-I).

### 6.1.2 Huhta Au deposit



In the Huhta deposit, the host rock foliation is cross-cut by auriferous quartz veins and actinolite-chlorite-sulfide veinlets (Fig. 5 A to D). The auriferous quartz-(sulfide) veins are a few millimetres to several centimetres wide and are usually deformed, showing undulose extinction of quartz and elongated, recrystallized quartz grains. Two mineralisation events are defined: (1) an As-Au event, subdivided into two stages; (1a) auriferous quartz-arsenide veins with löllingite containing invisible Au; (1b) auriferous quartz-sulfarsenide-sulfide veins defined by arsenopyrite with Au inclusions as well as pyrrhotite; (2) a sulfide event, locally overprinting the previous event, forming actinolite-chlorite-rich veinlets with chalcopyrite-pyrite-pyrrhotite-sphalerite (Fig. 2-B; Fig. 4-B).

Stage 1a is mostly cryptic and identified through rare löllingite cores preserved in stage 1b arsenopyrite (Fig. 2-B). Stage 1b is a continuation of stage 1a and is characterized by auriferous quartz veins with arsenopyrite and minor pyrrhotite. Arsenopyrite is euhedral to subhedral, locally forming clusters in veins (Fig. 5-C; -E to J). Locally it has pyrite, pyrrhotite, chalcopyrite, Au and gangue mineral inclusions (Fig. 5-G). It has low contents of Co and Ni (< 0.57 and < 0.38 wt.%, respectively) as well as trace concentrations of Sb, Bi, Cu, Hg, Ag and Zn (Table 1, ESM 2). Pyrrhotite occurs as patchy grains, generally in association with arsenopyrite and local chalcopyrite inclusions (Fig. 5-E). Gold occurs as disseminated, < 50µm inclusions in arsenopyrite, commonly together with Bi, hedleyite, pilsenite and maldonite, at a volumetric ratio of 1:10 (Fig. 5-G). Gold grains contain various amounts of Ag (avg. 21.10 wt.%), locally occurring as electrum. Invisible Au occurs rarely in chalcopyrite, pyrrhotite and pyrite (ESM 2). The veins have centimetre- to metre-scale hydrothermal alteration haloes characterized by a greenish-white bleached zone in the host rock (Fig. 5-A to D). Compared to unaltered rock, the bleached zone contains disseminated arsenopyrite and pyrite, and is depleted in mafic minerals, while plagioclase is replaced by sericite.

The mineralisation event 2 locally overprints the previous event, it is characterized by actinolite-chlorite-rich veinlets dominated by patchy pyrrhotite and porous pyrite grains with minor chalcopyrite and sphalerite. Pyrite has euhedral to patchy habits (Fig. 5-I and J) and locally fills fractures in arsenopyrite, replacing it along the rims (Fig. 5-I). Chalcopyrite and sphalerite are generally associated with pyrite, locally filling fractures (Fig. 5-F and J). The hydrothermal alteration halo in the host rock around actinolite-chlorite-rich veinlets is a few millimetres wide; it contains disseminated pyrrhotite, pyrite and chalcopyrite; plagioclase is replaced by sericite, biotite by chlorite, hornblende by fine-grained actinolite and ilmenite by titanite (Fig. 5-B-D).

## 6.2 Orogenic Au deposits with atypical metal associations



### 6.2.1 Jouhineva Au-Cu-Co-Ag deposit

Mineralisation at the Jouhineva deposit occurred in two events forming two vein sets: (1) an As-Au-Co-Ni event forming auriferous quartz-sulfarsenide-sulfide veins defined by arsenopyrite with Au inclusions and slight Ni and Co enrichment; and (2) a sulfide (Cu-Au) event, locally overprinting the previous event, forming auriferous actinolite-chlorite-rich veinlets with pyrite and chalcopyrite, along with free, native Au. A late barren alteration event overprints the mineralized veins, replacing chalcopyrite by bornite, digenite and tennantite (Fig. 2-C; Fig. 4-C).

The mineralisation event 1 is characterized by auriferous quartz-sulfide veins. The veins are a few millimetres to tens of centimetres wide and are usually deformed, showing undulose extinction of quartz, elongated quartz grains (Fig. 6-A to D). They mainly contain quartz with accessory apatite, biotite, K-feldspar, plagioclase, scheelite, titanite and zircon. Arsenopyrite is the main ore mineral with minor pyrite. Arsenopyrite is euhedral to subhedral, locally zoned and commonly forms clusters in veins (Fig. 6-A and D). They locally host Au, hedleyite, pilsenite, hessite and galena inclusions (Fig. 6-E and F). Arsenopyrite contains various amounts of Co and Ni (< 6.82 and < 0.54 wt.%, respectively) as well as traces of Sb, Bi, Cu, Hg, Ag and Zn (Table 1; ESM 2). Pyrite (Py1) is euhedral to subhedral with a spongy or porous texture (Fig. 6-G). Gold occurs as disseminated < 50µm inclusions in arsenopyrite. It represents up to 10 vol.% of the visible Au (Fig. 6-F) and occurs commonly together with < 50µm hedleyite, pilsenite, hessite and galena grains at a volumetric ratio of 1:10. The veins have millimetre- to centimetre-scale greenish-white hydrothermal alteration halos characterized by disseminated arsenopyrite and pyrite (Py1) and replacement of plagioclase by sericite and biotite by chlorite.

The mineralisation event 2 is characterized by actinolite-chlorite-sulfide veinlets locally cross-cutting and overprinting the previous auriferous quartz-sulfide veins. Sulfides are dominated by chalcopyrite and patchy pyrite (Py2) stretched along the foliation or filling fractures in quartz (Fig. 2-C; Fig. 6-G and H). Chalcopyrite occurs in significantly higher proportions than in the other deposits (Fig. 2), locally forming massive to semi-massive sulfide veins (Fig. 6-C and D). It contains Ag and shows localized enrichment in Au and Bi whereas pyrite contains traces of As, Cu, Co, Ni and Ag (Table 1; ESM 2). Locally, chalcopyrite and arsenopyrite have cubanite inclusions which have traces of As, Co, Ni and Ag (Table 1; ESM 2). Free native Au occurs as < 50 µm grains along with chalcopyrite in proximity of arsenopyrite in the quartz veins. It represents 90 vol.% of the visible Au (Fig. 6-I). The actinolite-chlorite-sulfide veinlets

have millimetre- to metre-scale, greenish-white, hydrothermal alteration halos characterized by disseminated chalcopyrite, pyrite (Py2) and rare Au, and replacement of biotite by chlorite and hornblende by fine-grained actinolite.

A late barren alteration event affected chalcopyrite, which is locally replaced by tennantite and Ag-rich minerals (pearceite, hessite, argentite) along newly formed fractures (Fig. 2-C; Fig. 6-E and H). Bornite and digenite locally replace chalcopyrite (Fig. 6-J). Tennantite contains < 4.08 wt.% Zn and traces of Co, Ni, Sb and Ag. Bornite contains traces of Ag, Sb, As, Bi, Au and Hg and digenite contains traces of Bi, Fe and Hg (Table 1 and ESM 2).

### 6.2.2 Kurula Au-Co deposit

In the Kurula deposit, the host rocks are cross-cut by sets of quartz-sulfide veins generally cross-cutting the foliation. The veins are a few millimetres to several centimetres wide and are generally sheared and locally folded (Fig. 7-A to D). They show internal deformation such as elongated, recrystallized quartz and quartz with undulose extinction. The mineralisation is the result of two events forming two sets of veins, locally overprinting each other: (1) an As-Au-Co-Ni event characterized by auriferous quartz-sulfide veins with arsenides and sulfarsenides; and (2) a sulfide event, locally overprinting the previous event, forming quartz-sulfide veins with chalcopyrite, pyrrhotite and sphalerite (Fig. 2-D; Fig. 4-D).

The mineralisation event 1 is subdivided into two stages: (1a) auriferous quartz veins with (Ni-Co-Fe) arsenides and invisible Au; and (1b) pyrite and replacement of arsenides by arsenopyrite (Apy1) with Au inclusions. Stage 1a is characterized by auriferous quartz veins with Ni-Co-Fe arsenides such as löllingite, clinosafflorite, safflorite, skutterudite and rammelsbergite (Fig. 2-D). The arsenides occur as < 1mm inclusions in stage 1b arsenopyrite (Apy1). The inclusions locally form a patchy assemblage with K-feldspar and arsenopyrite (Apy1) (Fig. 7-E). Löllingite contains little Co and Ni, safflorite has a heterogeneous composition and contains < 11.15 wt.% Co, < 2.28 wt.% Ni and traces of Sb, Bi, Cu, Hg, Ag and Zn and rammelsbergite contains traces of Sb, Bi, and Co and skutterudite traces of Sb, Bi, Cu, Hg and Ag (Table 1, ESM 2).

Stage 1b is continued prolongation from stage 1a and is characterized by arsenopyrite (Apy1) and pyrite (Py1) with minor Au, maldonite, Bi, hedleyite, pilsenite and molybdenite (Fig. 2-D). Arsenopyrite (Apy1) forms euhedral to subhedral grains, locally fractured and commonly forming clusters (Fig. 7-C and G). Locally, it contains inclusions of Ni-Co-Fe arsenides and gangue minerals as well as Au, Bi, hedleyite, pilsenite and maldonite inclusions (Fig. 7-E and H). It

is locally chemically zoned, two types are identified, one with low Ni and high Co content (< 5.95 wt.%) and another with slightly enriched Ni contents (< 0.94 wt.%, ESM 2). Arsenopyrite (Apy1) contains traces of Sb, Bi, Cu, Au, Hg, Ag and Zn (Table 1, ESM 2). Gold occurs as < 50µm inclusions in arsenopyrite (Apy1). The Au inclusions occur commonly together with Bi, hedleyite, pilsenite and maldonite at a volumetric ratio of 1:10. Gold grains contain small amounts of Ag, As, Fe and traces of Bi, Co, Cu, Ni, S (Table 1, ESM2). Where arsenopyrite (Apy1) contains Ni-Co-Fe arsenide cores, the inclusions tend to be concentrated at the contact between both minerals (Fig. 7-E). A second generation of arsenopyrite (Apy2) occurs locally as overgrowth on arsenopyrite (Apy1), generally with pyrite (Py1) (Fig. 7-F). Arsenopyrite (Apy2) is not chemically zoned and Co is below detection limit (Table 1, ESM 2). Pyrite (Py1) occurs as euhedral to subhedral deformed grains. Pyrite (Py1) shows porosity, gangue mineral inclusions and locally a spongy texture (Fig. 7-F). The gangue of the event 1 veins is composed of quartz, tourmaline, plagioclase, biotite, K-feldspar and accessory actinolite, apatite, scheelite, titanite and zircon. The host rock within a few centimetres of the mineralized hydrothermal veins contains hydrothermal tourmaline, sericite, chlorite and disseminated arsenopyrite and pyrite (Py1). Plagioclase is replaced by sericite and biotite by chlorite (Fig. 7-B).

The mineralisation event 2 is characterized by quartz-sulfide veins with chalcopyrite, pyrrhotite, sphalerite and pyrite (Py2), which locally cross-cut and overprint the veins of event 1 (Fig. 2-D). Chalcopyrite occurs as deformed grains and locally forms a patchy texture with sphalerite and pyrite (Py2) (Fig. 7-H and I). It locally contains pyrite (Py2), gangue mineral and rare Bi inclusions (Fig. 7-I). Pyrite (Py2) is pristine, euhedral to subeuhedral and locally replaces chalcopyrite (Fig. 7-I). Pyrrhotite occurs as spongy and porous deformed grains. It locally has pyrite, chalcopyrite and gangue mineral inclusions (Fig. 7-J). Chalcopyrite contains traces of Ag, Sb, Bi, Hg and Zn; pyrite contains traces of Cu, Hg and Zn; and pyrrhotite has traces of As and Au (Table 1, ESM 2). The host rock within a few centimetres of the mineralized hydrothermal veins contains hydrothermal tourmaline, sericite, chlorite and disseminated chalcopyrite, pyrrhotite and pyrite (Py2). Plagioclase and biotite are replaced by sericite and chlorite respectively.

## 6.3 ARSENOPYRITE GEOTHERMOMETRY

The arsenopyrite geothermometer from Kretschmar and Scott (1976) is applied to the arsenopyrite-bearing assemblages of the four deposits. Arsenopyrite shows a natural compositional heterogeneity compared to the theoretical As content (33.33 at.% As) and can contain significant amounts of Co, Ni, Sb, leading to anomalous temperature estimates (Sharp et al. 1985). All data has been carefully sorted and data with $Fe/(As+S)<0.5$ and/or $\Sigma(Co, Ni, Sb)> 1$ wt.% were removed (Kretschmar and Scott 1976).

### 6.3.1 Laivakangas Au deposit



Arsenopyrite in equilibrium with pyrrhotite and löllingite has an As content of 34.72 ± 0.48 at.% As (n=3) and yields an average temperature of 485 ± 25°C for the mineralisation event 2 (Fig. 8-A). Arsenopyrite only in equilibrium with löllingite has a consistent As content of 34.71 ± 0.50 at.% As (n=25) and thus yields the same temperature (Fig. 8-A).

### 6.3.2 Huhta Au deposit

Arsenopyrite is in equilibrium with pyrrhotite. Data from disseminated arsenopyrite in the hydrothermal alteration zone and arsenopyrite in a quartz vein are plotted (Fig. 8-B). Arsenopyrite from the quartz vein shows compositional zoning with the As content varying between 30.19 and 34.90 at.% As (Fig. 8-B'). This variation is either caused by changing conditions during deposition (Sharp et al. 1985) or by diffusion/remobilisation of As. This scattered data yields an average temperature of 475 ± 125°C (n=10) for the stage 1b of the mineralisation event 1. Arsenopyrite FEMO-2019-22-13b-22 (see Fig. 8-B and B') does not show evidence of remobilisation and is considered as reference value for the As content in arsenopyrite. The compositional data yields a temperature of 480 ± 40°C, which is close to the average temperature determined using all the data. Disseminated arsenopyrite, locally in equilibrium with pyrrhotite, yields a lower temperature of 380 ± 50°C, with a consistent As content (31.83 ± 0.35 at.% As; n=12).

### 6.3.3 Jouhineva Au-Cu-Co-Ag deposit

Arsenopyrite is in equilibrium with pyrite (Py1). However, arsenopyrite in direct contact with pyrite (Py1) has a Σ(Co, Ni, Sb) > 1 wt.% and cannot be used. Geothermometry using valid arsenopyrite data yields an average temperature of 495 ± 20°C for the mineralisation event 1 (Fig. 8-C; n=47). This temperature is obtained from arsenopyrite grains not in local equilibrium with pyrite (Py1). However, the As content in arsenopyrite is consistent (33.04 ± 0.40 at.% As) and there is no evidence for several generations of arsenopyrite and neither pyrrhotite nor löllingite are observed in the samples.

### 6.3.4 Kurula Au-Co deposit



Arsenopyrite (Apy1 and Apy2) are in equilibrium with pyrite. Arsenopyrite (Apy1) typically contains several wt.% of Co and Ni, preventing reliable temperature estimation. Due to the rare occurrence of arsenopyrite (Apy2), only one measurement matches all the required criteria with an As content of 32.09 at.% (Fig. 8-D'). The data yields a temperature of 430°C for the stage 1b of the mineralisation event 1 (Fig. 8-D).

## 6.4 Sulfur isotopes

The $\delta^{34}S$ signature of arsenopyrite, pyrrhotite, pyrite and chalcopyrite from the four deposits show a relatively wide range from +1.39 ‰ to +8.21 ‰ (Fig. 9; Table 2). This variation is rather deposit-related as mineralisation event or mineral-related as, within each deposit, arsenopyrite and sulfides forming during different events show a similar range in $\delta^{34}S$ (Table 2). A different $\delta^{34}S$ range is observed between the Laivakangas (+1.52-+3.17‰ $\delta^{34}S$), Huhta (+4.44-+6.55‰ $\delta^{34}S$), Jouhineva (+5.87-+8.21‰ $\delta^{34}S$) and Kurula deposits (+1.39-+3.17‰ $\delta^{34}S$, Table 2). Noticeably there is a marked difference in $\delta^{34}S$ between the Laivakangas and Kurula deposits, which have lighter $\delta^{34}S$ (+1.39-+3.17‰), and the Jouhineva and Huhta deposits, which have the heavier S isotopic composition (+4.44-+8.21‰).

# 7 Discussion

## 7.1 Multi-event orogenic Au deposits

The detailed characterisation of the paragenetic sequences of the Laivakangas, Huhta, Jouhineva and Huhta deposits highlights that orogenic Au mineralisation in the Pohjanmaa Belt is of a complex multi-event, multi-stage origin. Regionally, two main hydrothermal mineralisation events are defined, each with a specific metal association. Their respective intensity in the different deposits accounts for the bulk metal endowment and ultimately to the classification of each deposit as Au-only or orogenic Au with atypical metal association. The two main mineralisation events are: 1) an As-Au (Co, Ni) event in all four deposits, characterized by arsenides and/or sulfarsenides locally enriched in Ni and Co. Gold likely occurs as invisible Au in the arsenides and occurs as Au inclusions in sulfarsenides; 2) a sulfide event with Cu(-Au) mostly expressed at the Laivakangas and Jouhineva deposits. Event 2 is characterized by chalcopyrite and other sulfides and free, native Au in fractures of vein quartz and silicates, and locally as scarce Au inclusions in pyrrhotite and chalcopyrite.

### 7.1.1 Laivakangas Au deposit



The As-Au(-Co) mineralisation event 1, defined by auriferous quartz-arsenide veins, occurred close to the metamorphic peak at a temperature between 575 ± 50°C (Mäkelä 1984) and 485 ± 25°C, i.e. temperature of formation of arsenopyrite during the event 2 (Fig. 3; Fig. 8-A). Invisible Au (below 202 ppm in arsenides; ESM 2) is inferred to occur in Ni-Co-Fe arsenides based on petrological relationships between Ni-Co-Fe arsenides, replacing arsenopyrite (event 2) and Au inclusions (see next paragraph; Fig. 3-F to H). Furthermore, arsenopyrite is locally enriched in Ag which tends to be enriched alongside Au in arsenides and arsenopyrite (Lee et al. 2019). The limited extent of preserved arsenides and the relatively low Ni and Co content in replacing arsenopyrite account for the low bulk enrichment of Ni and Co at Laivakangas. Up to 90 % of the visible Au of the Laivakangas deposit is Au inclusions trapped almost exclusively in arsenopyrite and Ni-Co-Fe arsenide implying the mineralisation event 1 is the main Au stage.

The sulfide (Cu-Au) mineralisation event 2 is defined by new auriferous quartz-sulfide veins and by auriferous quartz-sulfarsenide-sulfide veins where it overprints the previous veins of the event 1 (see section 6.1.1). It is inferred to have occurred at 485 ± 25°C (arsenopyrite geothermometry; Fig. 8-A), which is supported by the chalcopyrite-pyrrhotite-cubanite assemblage that indicates temperatures of <500 °C (Yund and Kullerud 1966). The overprinting veins are characterized by the replacement of Ni-Co-Fe arsenide (event 1) by arsenopyrite (Fig. 2-A). Local enrichment in Co and Ni, Ni-Co-Fe arsenide cores and Au and Bi-(Te, Au, Ag, Cu) mineral inclusions in arsenopyrite (Fig. 3-F to H) are interpreted as showing the retrograde reaction of Ni-Co-Fe arsenide and pyrrhotite to arsenopyrite (1) (Neumayr et al. 1993; Tomkins and Mavrogenes 2001):

$$FeAs_2 + FeS + 0.5S_2 \rightarrow 2FeAsS \quad (1)$$

Pyrrhotite is rarely observed in assemblage with Ni-Co-Fe arsenide, although it is a necessary partner for the retrograde reaction. It is possible that pyrrhotite was completely consumed by the reaction. The reaction of Ni-Co-Fe arsenide with the higher $fS_2$ fluid of event 2 appears a better alternative which would be concomitant with sulfide precipitation (Barton 1969):

$$FeAs_2 + 2H_2S_{(aq)} + Fe^{2+}_{(aq)} \rightarrow 2FeAsS + 4H_{2(aq)} \quad (2)$$

Replacement of Ni-Co-Fe arsenide by arsenopyrite forces invisible Au as solid solution within the arsenides to exsolve as Au inclusion because Au is not well incorporated into arsenopyrite at temperatures above 300°C (Neumayr et al. 1993, based on Cathelineau et al. 1989; Tomkins and Mavrogenes 2001). The rare Au inclusions in chalcopyrite

and pyrrhotite as well as free, native Au grains indicate a new hydrothermal input of Au during the sulfide (Cu-Au) event 2 (Fig. 2-A; Fig. 3-K). The relative scarcity of pyrrhotite and chalcopyrite in the overprinting veins compared to the newly formed veins (see Fig. 4-A) is likely because most of the sulfidation was taken in converting the previous arsenides to arsenopyrites instead of forming new sulfides.

### 7.1.2 Huhta Au deposit

The As-Au mineralisation event 1 of the Huhta deposit is subdivided into two stages: an As-Au arsenide stage (1a) and an As-S-Au sulfarsenide stage (1b) (Fig. 2-B; Fig. 4-B). Stage 1a consists of quartz veins with a little löllingite possibly containing invisible Au, as indicated by its replacement by arsenopyrite containing Au inclusions. Stage 1b likely occurred on the early retrograde metamorphic path at 480 ± 40°C (arsenopyrite geothermometry; Fig. 8-B) after peak metamorphism (545 ± 30°C; Hölttä and Heilimo 2017). It is characterized by arsenopyrite with Au inclusions and rare löllingite cores (stage 1a), minor pyrrhotite and accessory chalcopyrite and pyrite (Fig. 2-B). Rare löllingite cores in arsenopyrite suggest that a portion of the arsenopyrite formed by replacement of the previous löllingite, either by reaction with a higher $fS_2$ fluid or by retrograde reaction between löllingite and pyrrhotite (Barton 1969; Tomkins and Mavrogenes 2001), as described above for the Laivakangas deposit. Au inclusions in löllingite-free arsenopyrite are explained either by complete replacement of löllingite or by co-precipitation of native Au and arsenopyrite from the stage 1b hydrothermal fluid (Fig. 5-G). The estimated temperature of formation for arsenopyrite of 480 ± 40°C is close to the estimated temperature of arsenopyrite formation for the Jouhineva deposit (470 - 495°C). Which suggest that stage 1b in the Huhta deposit is the equivalent of the mineralisation event 1 in the Jouhineva deposit. As the two deposits are located only 2.8 kilometres apart along the same structure, these similar temperatures indicate that arsenopyrite formed at similar timing on the retrograde metamorphic path. However, the two deposits show different metal enrichments, with no Ni and Co and significantly less Cu in the Huhta deposit than in Jouhineva deposit.

The mineralisation event 2 in the Huhta deposit is defined by pyrrhotite, pyrite, minor chalcopyrite and sphalerite in actinolite-chlorite-rich veinlets. It likely occurred during latest stages of retrograde metamorphism, under greenschist facies conditions, and appears to be Au barren (Fig. 2-B).

### 7.1.3 Jouhineva Au-Cu-Co-Ag deposit

The As-Au-Co(-Ni) mineralisation event 1 occurred during retrogression after peak metamorphism (545 ± 30°C; Hölttä and Heilimo 2017) at approx. 470-495°C (arsenopyrite geothermometry; Fig. 8-C). It is characterized by quartz

455 veins with arsenopyrite, with Au inclusions, and minor pyrite (Py1) (Fig. 2-C). Cobaltite is described in the literature

456 but has not been observed in this study due to sample bias (Geological Survey of Finland 2019b). However, as cobaltite
457 and arsenopyrite are both sulfarsenides with overlapping stability fields (Scharrer et al. 2019), both minerals likely
458 formed at similar conditions. Arsenopyrite contains on average 1.53 wt.% Co, which reflects the overall Co enrichment
459 of the deposit relative to Laivakangas and Huhta. The Cu-Au mineralisation event 2 is responsible for the main
460 hydrothermal input of Au, it is characterized by actinolite-chlorite-rich veinlets and major chalcopyrite, minor pyrite
461 (Py2), cubanite and free, native Au (Fig. 2-C). Mineralisation occurred during retrograde metamorphism at greenschist
462 facies conditions according to the mineral assemblage. The Jouhineva deposit has been proposed to be a Cu porphyry
463 deposit linked to the formation of the Rautio batholith and later overprinted by orogenic Au. This is unlikely as the
464 Rautio batholith formed at 1890-1880 Ma (Huhma 1986); i.e. before peak metamorphism (ca. 1880-1810 Ma; Hölttä
465 et al. 2019) and the hydrothermal mineralisation events occurred after metamorphic peak during retrograde terrane
466 exhumation.

467 ### 7.1.4 Kurula Au-Co deposit

468 The As-Au-Co-Ni mineralisation event 1 of the Kurula deposit is subdivided into two stages: an As-Au-Co-Ni
469 arsenide stage (1a) and an As-S(-Au) sulfarsenide stage (1b) (Fig. 2-D; Fig. 4-D). Stage 1a appears to have occurred after
470 the peak of metamorphism, which implies a temperature of formation between 620 ± 40°C (peak metamorphism
471 temperature; Hölttä and Heilimo 2017) and 430°C (stage 1b arsenopyrite geothermometry; Fig. 8-D). Nickel-Co-Fe
472 arsenides in veins and disseminated in the host rock result in significant endowment in Co and Ni relative to the other
473 deposits (Fig. 2-D). Nickel-Co-Fe arsenides are inferred to contain invisible Au, based on Au inclusions in replacing
474 arsenopyrite (Apy1, stage 1b) (Fig. 7-E).

475 Stage 1b is continuous to stage 1a and is characterized by replacement of Ni-Co-Fe arsenides (stage 1a) by
476 arsenopyrite (Apy1;Fig. 2-D). According to arsenopyrite geothermometry, it occurred during retrograde
477 metamorphism at 430°C (Fig. 8-D). The absence of pyrrhotite in the assemblage suggests that, like in the Laivakangas
478 deposit, arsenopyrite (Apy1) formed after reaction of Ni-Co-Fe arsenides with a higher $fS_2$ fluid (Barton 1969).
479 Arsenopyrite is the only sulfarsenide replacing the Ni-Co-Fe arsenides, the absence of cobaltite is likely caused by the
480 relative scarcity of skutterudite (Co-rich arsenide) compared to Fe-rich safflorite and löllingite in the arsenide
481 assemblage. The availability of Fe instead of sufficient Co led to formation of Co-rich arsenopyrite (Apy1) instead of

cobaltite. Limited metal input appears to be associated with the stage 1b in the Kurula deposit. The sulfide event 2 shows little evidence of Au enrichment (Fig. 2-D).



## 7.2 As-Au (Co, Ni) and Au-Cu mineralisation processes

Arsenopyrite of the Jouhineva deposit hosts fewer Au and Bi-(Te, Au, Ag, Cu) mineral inclusions than the arsenopyrite that replaced arsenides at the other deposits during mineralisation event 1. This difference is likely caused by the origin of the arsenopyrite. Indeed, arsenides such as löllingite are commonly enriched in Au and can accommodate Au up to several hundred ppm in their crystal lattice (Neumayr et al. 1993). On the other hand, arsenopyrite cannot incorporate Au efficiently (less than 10 ppm) in its structure at temperatures above 300°C (after Neumayr et al. 1993, based on Cathelineau et al. 1989). Thus, during replacement of arsenides by arsenopyrite, Au cannot stay in the crystal lattice and Au and Bi-(Te, Au, Ag, Cu) mineral inclusions will form in arsenopyrite. Conversely, arsenopyrite that precipitates directly from a fluid or directly formed by fluid-rock reaction contains fewer Au and Bi-(Te, Au, Ag, Cu) mineral inclusions as they do not form from an Au-rich precursor (i.e. arsenides).

The stability of arsenides and sulfarsenide, in hydrothermal systems is highly sensitive to $fS_2$ and $fO_2$ (e.g. Scharrer et al. 2019). Arsenides usually form by reduction of an oxidized, As-rich and S-poor fluid. Already small amounts of S will directly lead to sulfarsenide formation (Scharrer et al. 2019). The main mechanisms proposed for fluid reduction are: dissolution of graphite or $Fe^{2+}$-bearing minerals and/or pre-existing sulfides from the metamorphic host rocks as well as influx of hydrocarbons or $H_2S$ (Kissin 1993; Kreissl et al. 2018; Markl et al. 2016). Metamorphic fluids related to orogenic Au deposits generally contain significant amounts of $H_2S$ (Goldfarb and Groves 2015), which is likely to inhibit arsenide formation (Scharrer et al. 2019). The Jouhineva and the Huhta deposits show no to very scarce arsenide, indicating that conditions were not sufficiently reduced to compensate for the relatively high $fS_2$ of the fluids. In comparison, the Laivakangas and the Kurula deposits, had lower $fS_2$ than Jouhineva and Huhta (Fig. 8), favouring arsenide formation. The host rock of the Kurula deposit contains graphite which likely buffers the system to reducing conditions, promoting Fe-Ni-Co arsenide formation. Hence, $fS_2$ and redox conditions are important for the formation of arsenides over sulfarsenides and entrapment of Au during the regional As-Au(Co-Ni) mineralisation event 1. Cobalt and Ni content is more likely controlled by the original Co and Ni content in the fluid, as they can precipitate in arsenides and sulfarsenides over a broad range of $fS_2$ and redox conditions (Scharrer et al. 2019). Higher solubility of Co as chloride complex than Ni at a given salinity explains the higher proportion of Co relative to Ni in the studied orogenic Au deposits with atypical metal associations (Brugger et al. 2016).

Copper enrichment in the investigated deposits is related to the Cu(-Au) mineralisation event 2, expressed by sulfide minerals, mostly chalcopyrite. This event occurs systematically later and independently from the As-Au (Co, Ni) regional mineralisation event 1. Chalcopyrite is a minor to trace mineral in many orogenic Au deposits and has been observed in each of the studied deposits. Chalcopyrite, however, generally occurs as a minor mineral (Huhta, Kurula, Laivakangas) except in the Jouhineva deposit where it is present in significantly larger quantities (Fig. 6-C and D). Gold enrichment may occur in the form of free, native grains or as rare inclusions in chalcopyrite and pyrrhotite (Laivakangas, Jouhineva). The threshold for the classification of orogenic Au deposits as atypical Au-Cu deposits is arbitrary and is related to economic, rather than geological considerations.

## 7.3 CONSTRAINTS ON THE SOURCE AND FLUIDS

The studied Au deposits of the Pohjanmaa Belt formed through two hydrothermal events during the Fennoscandian orogeny, shortly after peak metamorphism at amphibolite facies and during retrograde evolution in greenschist facies. Although the deposits share a similar succession of mineralisation events, they do not show the same metal endowment indicating possibly either different mineralizing conditions, deposit type or different fluid sources.

### 7.3.1 Are atypical orogenic Au deposits related to porphyry mineralisation ?

The relative Cu-enrichment in the orogenic Au deposits of the Laivakangas Au-Cu metallogenic area has been suggested to be partly related to a porphyry style Cu±Au mineral system, overprinted by orogenic Au mineralisation (Eilu 2015, Geological Survey of Finland 2019b). Cu-Au porphyry deposits linked to the Svecofennian orogeny have been identified in the Pohjanmaa belt (Kopsa Cu-Au deposit; Gaál and Isohanni 1979); although, the studied orogenic deposits show very little similarities. The Kopsa deposit is located in the south-east of the study area, within the Hitura metallogenic area (Fig. 1- A). It is hosted in already metamorphosed host rocks, where the mineralisation is occurring as a quartz vein stockwork with major chalcopyrite, arsenopyrite and pyrrhotite. In addition, this stockwork is surrounded by a broad zone of disseminated pyrite-pyrrhotite and has been altered over a width of several hundred metres to a potassic assemblage with a propylitic halo (Gaál and Isohanni, 1979). Such extensive alteration and disseminated mineralisation are not observed in the studied orogenic Au deposits. The typical features of porphyry-related deposits can however be affected by later metamorphic events, making them harder to identify as such. Examples of porphyry-related deposits metamorphosed to greenschist-lower amphibolite facies (e.g. Chapada Cu-Au

deposit in Brazil, Oliveira et al. 2016; Chibougamau Cu-Au(-Mo) mining district, Pilote et al. 1995, Lac Troilus in Canada, Fraser 1993) still display a recognizable succession of alteration haloes, despite the modified mineralogy. The original argillic and potassic alteration are identified by a metamorphic assemblage rich in kyanite and biotite, respectively, and disseminated sulfides are observed in the host rock (Fraser 1993; Oliveira et al. 2016). In the case of the Chibougamau mining district, the porphyry-related deposits were metamorphosed at greenschist facies (Jolly 1974) and contain locally late auriferous hydrothermal breccia, interpreted as orogenic Au overprint and/or remobilisation during metamorphism (Guha and Koo 1975; Mathieu et al. 2019). However, the alteration halo is still identifiable by high K values in the whole rock geochemistry as well as mineral assemblage in the veins specific to magmato-hydrothermal systems (e.g. albite and magnetite) (Mathieu 2019; Mathieu et al. 2019).

By contrast, the rather narrow hydrothermal alteration zones and the mineralogy of the host rocks observed in the studied deposits are characteristic of orogenic Au deposits (Eilu and Groves, 2001) and are not consistent with the features observed in porphyry-related deposits, metamorphosed or not. Additionally, the Cu(-Au) mineralisation observed in the studied deposits systematically post-dates the As-Au (Co, Ni) mineralisation event and does not fit with the model of overprinted Cu ± Au porphyry. If the studied deposits are not overprinted Cu ± Au porphyry, we do not rule out that the Cu enrichment observed during the Cu(-Au) event could have a magmatic source. Indeed, during the time span of mineralisation, there is syn-orogenic magmatic activity in the Svecofennian orogen that could have led to production of Cu(-Au) rich magmatic fluids (Nironen 2005; Peltonen 2005).

### 7.3.2 Potential of metamorphic fluids for atypical metal enrichment in orogenic Au deposits

Although local variations in redox conditions affects the mineralogy (arsenides vs sulfarsenides) the diversity in metal enrichment between the studied deposits and the mineralisation events most likely imply that the respective ore fluids had differing metal contents during the metallogenic evolution. While it has been shown by Ridley and Diamond (2000) that ore fluids forming orogenic Au deposits usually display very similar geochemistry due to homogenisation by interaction with the different wall rocks between the source area and the depositional site, several recent studies underline how the lithological diversity of the source rocks impacts the metal content of the fluids during metamorphic devolatilisation (Patten et al. 2020, 2022; Zhao et al. 2011). The variability in metal enrichment between the deposits and mineralisation events can be a consequence of the dynamic nature of orogenic processes, during which different lithological units follow different metamorphic paths (e.g. Kolb et al. 2000, 2015), leading to

564 the generation of metamorphic fluids with diverse metal association (e.g. Patten et al. 2022). Cobalt, Cu and Ni can be

565 transported in hydrothermal fluids as chloride complexes at salinities as low as ca. 3 wt.% NaCl at 440°C, which is
566 characteristic of orogenic Au ore fluids (Liu et al. 2011, 2012). The presence of meta-evaporite, although not reported
567 in the Pohjanmaa Belt, can lead to higher fluid salinity, enhancing base metal mobilisation from the source zones
568 (Brugger et al. 2016; Qiu et al. 2021; Vasilopoulos et al. 2021). The $\delta^{34}S$ signature of the studied deposits (Fig. 9) is
569 within the range of metamorphic fluids (+0 to +9 ‰; McCuaig and Kerrich 1998). The Laivakangas and Kurula deposits,
570 however, have a low $\delta^{34}S$ range (+1.39 to +3.17‰; Table 2; Fig. 9), relative to the Jouhineva and Huhta deposits (+4.44
571 to +8.21‰; Table 2; Fig. 9). Several processes can affect the S isotopic signature during precipitation, such as
572 temperature, S species, pH and $fO_2$, (e.g. Hutchison et al. 2020; Ohmoto 1986). The overall similar precipitation
573 conditions during the sulfide mineralisation event 2 (greenschist facies metamorphic conditions) at the different
574 deposits, however, suggest that the differences in $\delta^{34}S$ are related to different isotopic fluid signature, buffered at
575 depth by different lithologies and along the transport path, rather than precipitation mechanisms.

576 The lithological variability in the source can have an important control on base metal endowment in orogenic Au
577 deposits. Although Au, As and S can be readily mobilized from both meta-sedimentary and meta-volcanic rocks (Large
578 et al. 2011; Patten et al. 2020, 2022; Pitcairn et al. 2006, 2021) the relative proportion of meta-sedimentary rocks
579 (including meta-evaporite) to meta-volcanic rocks in metamorphic fluid production zones likely control the content of
580 base metals available for ore formation (Patten et al. 2022). Local and transient changes in the metal content of the
581 fluid over time can explain the small-scale variation of metal association between deposits belonging to the same
582 structural system (e.g. Jouhineva and Huhta deposits).

# 583 8 CONCLUSION

584 The investigation of four orogenic Au deposits from the Pohjanmaa Belt with different metal association allows
585 a better understanding of the parameters controlling atypical base metal enrichment in orogenic Au deposits. The
586 Laivakangas, Huhta, Jouhineva and Kurula deposits formed by multiple hydrothermal mineralisation during two main
587 regional-scale auriferous events: (1) a ubiquitous As-Au (Co, Ni) event close to peak metamorphism inamphibolite
588 facies, where Au is likely trapped as invisible Au in arsenides or co-precipitated as inclusions in arsenopyrite, (2) a Cu(-
589 Au) sulfide event on the retrograde metamorphic path in greenschist facies where Au forms free, native grains along
590 with chalcopyrite. Importantly, the different base metals in the atypical orogenic Au deposits of the Pohjanmaa Belt

591 are not introduced simultaneously in the studied deposits. Our data reveal that Ni and Co are enriched during the early

592 hydrothermal stages, while Cu was introduced later in the metallogenic evolution. The relative intensity of each
593 mineralisation event can eventually control the metal endowment resulting in either classic orogenic Au or Au-Cu, Au-
594 Co and Au-Cu-Co deposits. Additionally, redox conditions and S fugacity appear to be an important parameter to
595 enhance Au grades during the mineralisation event 1, as Ni-Co-Fe arsenides can trap more Au than arsenopyrite.
596 Replacement of Ni-Co-Fe arsenides by arsenopyrite leads to formation of Au inclusions, which are easier to recover
597 during ore processing than invisible Au.

## 598 9 ACKNOWLEDGMENTS

599 We would like to thank Thomas Wenzel and Sebastian Staude from Eberhard Karls University of Tübingen for
600 assistance with SEM analysis, Otsogold for providing support and access to samples of the Laivakangas mine, the
601 Geological Survey of Finland (GTK) for granting access to the national drill core archive in Loppi and the Federal
602 Institute for Geosciences and the Federal Institute for Geosciences and Natural Resources (BGR) for funding. This
603 project was also supported by the OroTECT project (Academy of Finland grant No. 315188) in accordance with the
604 agreement between the Academy of Finland and DAAD. The authors would like to thank the reviewers and the editor
605 for their helpful and constructive comments.

606

## 9.1 TABLE CAPTION



Table 1 – Electron microprobe data of main ore minerals of the Laivakangas, Jouhineva, Huhta and Kurula deposits (see ESM 2 for detailed data)

Table 2 – Summary of S isotope data on sulfides of the Laivakangas, Jouhineva, Huhta and Kurula deposits (see ESM 3 for detailed data)

## 9.2 FIGURE CAPTIONS

Fig. 1- Geological setting (for location in Finland, see inset in A; CFGC: Central Finland Granitoid Complex; CLGB: Central Lapland Greenstone Belt; CLGC: Central Lapland Granitoid Complex; HB: Häme Belt; KB: Kuusamo Belt; PB: Peräpohja Belt; PiB: Pirkanmaa Belt; PoB: Pohjanmaa Belt; RLSZ: Raahe-Ladoga Shear Zone ; SB: Savo Belt; TB: Tampere Belt; UB: Uusimaa Belt; VB: Vaasa Batholith ). (A) Geological map of the Pohjanmaa Belt showing the metallogenic areas and major deposits (Y.f = Ylivieska field; E.f = Evijärvi field) (after Eilu et al. 2012); (B) Local geology of the Laivakangas deposit (Au); (C) Local geology of the Jouhineva deposit (Au-Cu-Co-Ag) and the Huhta deposit (Au); (D) Local geology of the Kurula deposit (Au-Co). Maps modified from Bedrock of Finland, DigiKP.

Fig. 2- (A) Paragenetic sequence of the Laivakangas deposit; (B) Paragenetic sequence of the Huhta deposit. Abbreviations as in previous figures; (C) Paragenetic sequence of the Jouhineva deposit; (D) Paragenetic sequence of the Kurula deposit. Abbreviations as in Fig. 3; Bi = native bismuth; Cov = covellite; Csf = clinosafflorite; Dg = digenite; Gn = galena; Hdl = hedleyite; Hs = hessite; Mdn = maldonite; Mol = molybdenite; Psn = pilsenite; Rbg = rammelsbergite; Sf = safflorite; Skt = skutterudite; Sp = sphalerite; Ten = tennantite.

Fig. 3- Representative ore samples from the Laivakangas deposit. (A-E) Auriferous quartz veins with arsenides, sulfarsenides and sulfides; (F) Co-rich arsenopyrite containing a clinosafflorite core, Au and Bi-(Te, Au, Ag, Cu) grains; (G) Detail of arsenopyrite with löllingite core and Au-rich and Bi-(Te, Au, Ag, Cu) grains; (H) Back-scattered electron-image (BSE-image) of Co-rich arsenopyrite with a clinosafflorite core and native Au and Bi grains; (I) Fractured arsenopyrite with cubanite along fractures, surrounded by pyrite (Py1), chalcopyrite and cubanite. Bornite replaces chalcopyrite. Au and Bi-(Te, Au, Ag, Cu) grains in arsenopyrite, along fractures and as free grains in the gangue; (J) Cubanite lamellae in chalcopyrite with pyrrhotite and pyrite (Py1); (K) Trail of Au and chalcopyrite in quartz vein. Abbreviations: Apy = arsenopyrite; Asn = Ni-Co-Fe arsenide; Au = gold; BiTe = Bi-(Te, Au, Ag, Cu) = bismuth, hedleyite,

633 pilsenite, hessite, wittichenite, volynskite, maldonite; Bn = bornite; Ccp = chalcopyrite; Chl = chlorite; Csf =

634 clinosafflorite; Cbn = cubanite; Lo = löllingite; Po = pyrrhotite; Py = pyrite; Qz = quartz.

635 Fig. 4- (A) Summary of the hydrothermal veins and alteration zones in the Laivakangas deposit. (1) Mineralisation event
636 1, quartz veins with löllingite and other Ni-Co-Fe arsenides with invisible Au. Hydrothermal biotite-(Ni-Co-Fe) arsenide
637 alteration zone along vein selvedges; (2) Mineralisation event 2, arsenide is replaced by arsenopyrite with Au
638 exsolutions in overprinted event 1 veins; chalcopyrite, pyrrhotite, pyrite (Py1), and free, native Au grains in event 2
639 veins. Hydrothermal sericite-chlorite alteration zone along vein selvedges; Late alteration event forming chlorite-
640 quartz veinlets with pyrite (Py2, Py3) and bornite. Abbreviations as in previous figures. (B) Summary of the
641 hydrothermal veins and alteration zones of the Huhta deposit. (1) Stage 1a of the mineralisation event 1, quartz veins
642 containing little löllingite; (2) Stage 1b of the mineralisation event 1, quartz veins containing pyrrhotite and
643 arsenopyrite with Au inclusions replacing löllingite. Local hydrothermal sericite-arsenopyrite-pyrrhotite alteration
644 zone along vein selvedges; (3) Mineralisation event 2, actinolite-chlorite-rich veinlets with pyrrhotite, pyrite and minor
645 chalcopyrite. Abbreviations as in previous figures. (C) Summary of the hydrothermal veins and alteration zones in the
646 Jouhineva deposit. (1) Mineralisation event 1, quartz veins with arsenopyrite and Au inclusions, and pyrite (Py1);
647 hydrothermal sericite-chlorite-arsenopyrite-pyrite (Py1) alteration zone; (2) Mineralisation event 2, actinolite-chlorite-
648 rich veinlets with chalcopyrite and pyrite (Py2) cross-cut event 1 quartz veins and host rock. Free native Au grains occur
649 with chalcopyrite; Late alteration event replacing chalcopyrite by bornite and digenite. Abbreviations as in previous
650 figures. (D) Summary of the hydrothermal veins and alteration zones in the Kurula deposit. (1) Stage 1a of the
651 mineralisation event 1, quartz veins with Ni-Co-Fe arsenides containing invisible Au. Hydrothermal tourmaline-biotite
652 alteration zone with accessory (Ni-Co-F) arsenides; (2) Stage 1b of the mineralisation event 1, pyrite (Py1) and
653 arsenopyrite (Apy1) with Au inclusions replace the arsenides (stage 1a). Sericite-chlorite alteration along veins
654 selvedges and local disseminated arsenopyrite and pyrite in the hydrothermal alteration zone; (3) Mineralisation event
655 2, quartz veins with chalcopyrite, pyrrhotite and accessory sphalerite. Pyrite (Py2) locally replaces chalcopyrite. Local
656 disseminated chalcopyrite in the hydrothermal alteration zone. Abbreviations as in previous figures.

657 Fig. 5- Representative ore samples of the Huhta deposit. (A-D) Auriferous quartz veins with arsenopyrite, pyrite,
658 pyrrhotite and hydrothermal sericite-chlorite alteration halos; (E) Arsenopyrite and pyrrhotite in quartz vein; (F) BSE-
659 image of arsenopyrite with chalcopyrite fracture-filling; (G) BSE-image of fractured arsenopyrite showing Au, Bi,
660 hedleyite and pilsenite inclusions. Pyrite and chalcopyrite fill fractures and porosity; (H) Quartz vein with arsenopyrite

(stage 1b) cross-cut by actinolite-chlorite-rich veinlet with pyrite (event 2). Hydrothermal sericite-chlorite-arsenopyrite alteration zone in meta-tonalite along the vein selvedges; (I) BSE-image of fractured arsenopyrite with euhedral pyrite replacing arsenopyrite along the rims and filling the fractures; (J) Actinolite-chlorite-rich veinlet with pyrite and sphalerite in quartz vein with arsenopyrite. Abbreviations as in previous figures; Chl = chlorite; Hdl = hedleyite; Psn = pilsenite; Ser = sericite.



Fig. 6- Representative ore samples of the Jouhineva deposit. (A-D) Mineralized quartz veins with arsenopyrite, chalcopyrite, pyrite, digenite and bornite; (E) BSE-image of arsenopyrite containing Au, hedleyite, hessite, cubanite, chalcopyrite and bornite inclusions. Arsenopyrite shows compositional zoning; (F) Gold and hedleyite inclusions in arsenopyrite; (G) Spongy and fractured pyrite (Py1) with pristine pyrite (Py2) and chalcopyrite; (H) Spongy pyrite with chalcopyrite being replaced by tennantite along fractures and porosity; (I) Disseminated free, native Au and chalcopyrite with arsenopyrite; (J) Quartz vein with pyrite and disseminated arsenopyrite and chalcopyrite. Bornite and digenite replace chalcopyrite. Abbreviations as in previous figures.

Fig. 7- Representative ore samples of the Kurula deposit. (A-D) Mineralized quartz veins with arsenopyrite, pyrrhotite and chalcopyrite. (E) BSE-image of arsenopyrite (Apy1) containing Ni-Co-Fe arsenide inclusions. Ni-Co-Fe arsenides form a patchy assemblage with arsenopyrite and K-feldspar. Pilsenite is disseminated in arsenopyrite (Apy1) and Ni-Co-Fe arsenides; (F) BSE-image of fractured arsenopyrite (Apy1 and Apy2) and pyrite (Py1) in quartz vein. Arsenopyrite (Apy1) shows a tone contrast linked to variability in Co content; (G) BSE-image of arsenopyrite (Apy1) cluster with chalcopyrite and pyrite (Py1) in quartz vein. Uraninite forms inclusions in sulfides and gangue minerals; (H) BSE-image of fractured arsenopyrite (Apy1) with safflorite inclusion. Gold and Bi occur at the contact between safflorite and arsenopyrite (Apy1). Patchy chalcopyrite-sphalerite assemblage rims arsenopyrite (Apy1), Bi forms inclusions in chalcopyrite; (I) Chalcopyrite and euhedral pyrite (Py2) in deformed quartz vein; (J) Arsenopyrite (Apy1) and spongy pyrrhotite with chalcopyrite inclusion in quartz vein. Abbreviations as in previous figures; Bt = biotite Csf = clinosafflorite; K-Fsp = K-feldspar; Tur = tourmaline.

Fig. 8- Arsenopyrite geothermometry. (A) Laivakangas deposit; (B) Huhta deposit, analysis 22-13b-22 is considered representative of the arsenopyrite As content; (B') BSE-image of a zoned arsenopyrite in equilibrium with pyrrhotite. Contrast has been increased. The arsenopyrite grain shows patchy As-poor zones in the centre and at the rim of the grain; (C) Jouhineva deposit; (D) Kurula deposit and (D') arsenopyrite 2 in equilibrium with pyrite.

Fig. 9- Range of $\delta^{34}S$ in sulfides of the Laivakangas, Jouhineva, Huhta and Kurula ores (see ESM 2 for data).



# 10 REFERENCES


Barton PB (1969) Thermochemical study of the system Fe-As-S. Geochimica et Cosmochimica Acta 33:841–857

Bedrock of Finland – DigiKP. Digital map database [Electronic resource]. Espoo: Geological Survey of Finland [referred 16.08.2022]. Version 2.1.

Bektas R, Vathavooran A (2019) Laiva, Finland NI 43-101 Resource Update

Brugger J, Liu W, Etschmann B, Mei Y, Sherman DM, Testemale D (2016) A review of the coordination chemistry of hydrothermal systems, or do coordination changes make ore deposits? Chemical Geology 447:219–253

Cathelineau M, Boiron M-C, Holliger P, Marion P, Denis M (1989) Gold in Arsenopyrites: Crystal Chemistry, Location and State, Physical and Chemical Conditions of Deposition. In: Keays RR, Ramsay WRH, Groves DI (eds) The Geology of Gold Deposits. Society of Economic Geologists, pp 328–341

Chopin F, Korja A, Nikkilä K, Hölttä P, Korja T, Abdel Zaher M, Kurhila M, Eklund O, Rämö OT (2020) The Vaasa Migmatitic Complex (Svecofennian Orogen, Finland): Buildup of a LP-HT Dome During Nuna Assembly. Tectonics 39

Eilu P, Groves DI (2001) Primary alteration and geochemical dispersion haloes of Archaean orogenic gold deposits in the Yilgarn Craton: the pre-weathering scenario. GEEA 1:183–200Eilu P (2015) Overview on Gold Deposits in Finland. In: Mineral Deposits of Finland. Elsevier, pp 377–410

Eilu P, Ahtola T, Äikäs O, Halkoaho T, Heikura P, Hulkki H, Iljina M, Juopperi H, Karinen T, Kärkkäinen N, Konnunaho J, Kontinen A, Kontoniemi O, Korkiakoski E, Korsakova M, Kuivasaari T, Kyläkoski M, Makkonen H, Niiranen T, Nikander J, Nykänen V, Perdahl J-A, Pohjolainen E, Räsänen J, Sorjonen-Ward P, Tiainen M, Tontti M, Torppa A, Västi K (2012) Metallogenic areas in Finland. In: Eilu P (ed) Mineral deposits and metallogeny of Fennoscandia. Geological Survey of Finland, Espoo, pp 207–342

Eilu P (2015) Overview on Gold Deposits in Finland. In: Mineral Deposits of Finland. Elsevier, pp 377–410

Fraser RJ (1993) The Lac Troilus gold-copper deposit, northwestern Quebec; a possible Archean porphyry system. Economic Geology 88:1685–1699

Gaal G, Isohanni M (1979) Characteristics of igneous intrusions and various wall rocks in some Precambrian porphyry copper-molybdenum deposits in Pohjanmaa, Finland. Economic Geology 74:1198–1210

715 Gaál G, Sundblad K (1990) Metallogeny of gold in the Fennoscandian Shield. Mineralium Deposita 25 (Suppl):S 104 - S
716 114

717 Gebre-Mariam M, Hagemann SG, Groves DI (1995) A classification scheme for epigenetic Archaean lode-gold deposits.
718 Mineralium Deposita:408–410

719 Geological Survey of Finland (2019a) Huhta. Mineral Deposit Report n° 446

720 Geological Survey of Finland (2019b) Jouhineva. Mineral Deposit Report n° 309

721 Geological Survey of Finland (2019c) Kurula. Mineral Deposit Report n° 307

722 Geological Survey of Finland (2019d) Laivakangas. Mineral Deposit Report n° 298

723 Goldfarb RJ, Groves DI, Gardoll S (2001) Orogenic gold and geologic time: a global synthesis. Ore Geology Reviews
724 18:1–75

725 Goldfarb RJ, Baker T, Dubé B, Groves DI, Hart CJR, Gosselin P (2005) Distribution, Character, and Genesis of Gold
726 Deposits in Metamorphic Terranes. In: Hedenquist JW (ed) Economic geology: One hundredth anniversary
727 volume: 1905-2005. Society of Economic Geologists, Inc, Littleton, CO, pp 407–450

728 Goldfarb RJ, Groves DI (2015) Orogenic gold: Common or evolving fluid and metal sources through time. Lithos 233:2–
729 26

730 Groves DI, Goldfarb RJ, Gebre-Mariam M, Hagemann SG, Robert F (1998) Orogenic gold deposits: A proposed
731 classification in the context of their crustal distribution and relationship to other gold deposit types. Ore Geology
732 Reviews 13:7–27

733 Guha J, Koo J (1975) Role of Fluid State Mobilisation during Metamorphism of the Henderson Ore Bodies,
734 Chibougamau, Quebec, Canada. Can. J. Earth Sci. 12:1516–1523

735 Haapala I, Rämö OT (2015) Mineral Deposits Related to Granitic Rocks. In: Mineral Deposits of Finland. Elsevier, pp
736 531-556

737 Hanski E, Huhma H (2005) Central Lapland Greenstone Belt. In: Lehtinen M, Nurmi PA, Rämö OT (eds) Precambrian
738 geology of Finland: Key to the evolution of the Fennoscandian shield, 1. ed. Elsevier, Amsterdam, pp 139–194

739 Haverinen J (2020) Evaporites in the Central Lapland Greenstone Belt. M.Sc. thesis, University of Helsinki

740 Hölttä P, Heilimo E (2017) Metamorphic map of Finland. In: Nironen M (ed) Bedrock of Finland at the scale 1:1 000
741 000: Major stratigraphic units, metamorphism and tectonic evolution. Geological Survey of Finland, Espoo, pp 77–
742 128

Hölttä P, Huhma H, Lahaye Y, Mänttäri I, Lukkari S, O'Brien H (2019) Paleoproterozoic metamorphism in the northern Fennoscandian Shield: age constraints revealed by monazite. International Geology Review 30:1–28

Huhma H (1986) Sm-Nd, U-Pb and Pb-Pb isotopic evidence for the origin of the Early Proterozoic Svecokarelian crust in Finland. Bulletin

Hutchison W, Finch AA, Boyce AJ (2020) The sulfur isotope evolution of magmatic-hydrothermal fluids: insights into ore-forming processes. Geochimica et Cosmochimica Acta 288:176–198

Isohanni M (1984) Malminetsintätyöt Kalajoen Jouhinevalla vuosina 1978 - 1983 (in Finnish). Report of Investigation

Jolly W.T.; Regional metamorphic zonation as an aid in study of Archean terrains; Abitibi region, Ontario. The Canadian Mineralogist 1974;; 12 (7): 499–508.

Kähkönen Y (2005) Svecofennian supracrustal rocks. In: Lehtinen M, Nurmi PA, Rämö OT (eds) Precambrian geology of Finland: Key to the evolution of the Fennoscandian shield, 1. ed. Elsevier, Amsterdam, pp 343–406

Kissin SA (1993) The geochemistry of transport and deposition in the formation of five-element (Ag-Ni-Co-As-Bi) veins. In: Maurice YT (ed) Proceedings of the Eighth Quadrennial IAGOD Symposium: Held in Ottawa, Canada, August 12-18, 1990 / papers presented at the symposium on topics related to general problems on the genesis of ore deposits and on studies of the ore geology of specific districts or deposits. E. Schweizerbart, Stuttgart

Kiuttu L (2020) Petrology and mineral chemistry of the Ylivieska gabbro-peridotite intrusion: constraints on the petrogenesis and Ni sulfide ore potential. Master's thesis

Kolb J, Meyer FM, Kisters AFM (2000) Amphibolite facies gold mineralisation at Renco, Zimbabwe: Conditions of ore formation. In: Rammlmair D (ed) Applied mineralogy in research, economy, technology, ecology and culture: Proceedings of the sixth International Congress on Applied Mineralogy / Göttingen, Germany, 17-19 July 2000 / ICAM 2000. A.A. Balkema, Rotterdam, Brookfield, pp 355–357

Kolb J, Dziggel A, Bagas L (2015) Hypozonal lode gold deposits: A genetic concept based on a review of the New Consort, Renco, Hutti, Hira Buddini, Navachab, Nevoria and The Granites deposits. Precambrian Research 262:20–44

Korja A, Lahtinen R, Nironen M (2006) The Svecofennian orogen: a collage of microcontinents and island arcs. Geological Society, London, Memoirs 32:561–578

Kreissl S, Gerdes A, Walter BF, Neumann U, Wenzel T, Markl G (2018) Reconstruction of a >200 Ma multi-stage "five element" Bi-Co-Ni-Fe-As-S system in the Penninic Alps, Switzerland. Ore Geology Reviews 95:746–788

Kretschmar U, Scott SD (1976) Phase relations involving arsenopyrite in the system Fe-As-S and their application. Canadian Mineralogist 14:364–386

Kurhila M, Molnár F, O'Brien H, Tiljander M, Johanson B, Middleton A (2017) U-Pb dating of hydrothermal monazite and xenotime from the Levijärvi-Loukinen gold deposit, Central Lapland Greenstone Belt, Northern Finland. In: Hölttä P, Nenonen K, Eerola T (eds) Guide 63: Abstract Book, pp 56–57

Laajoki K (2005) Karelian supracrustals rocks. In: Lehtinen M, Nurmi PA, Rämö OT (eds) Precambrian geology of Finland: Key to the evolution of the Fennoscandian shield, 1. ed. Elsevier, Amsterdam, pp 279–342

Lahtinen R, Huhma H, Kousa J (2002) Contrasting source components of the Paleoproterozoic Svecofennian metasediments: Detrital zircon U–Pb, Sm–Nd and geochemical data. Precambrian Research 116:81–109

Lahtinen R, Korja A, Nironen M (2005) Paleoproterozoic tectonic evolution. In: Lehtinen M, Nurmi PA, Rämö OT (eds) Precambrian geology of Finland: Key to the evolution of the Fennoscandian shield, 1. ed. Elsevier, Amsterdam, pp 481–532

Lahtinen R, Johnston ST, Nironen M (2014) The Bothnian coupled oroclines of the Svecofennian Orogen: a Palaeoproterozoic terrane wreck. Terra Nova 26:330–335

Large RR, Bull SW, Maslennikov VV (2011) A Carbonaceous Sedimentary Source-Rock Model for Carlin-Type and Orogenic Gold Deposits. Economic Geology 106:331–358

Lawrence DM, Treloar PJ, Rankin AH, Harbidge P, Holliday J (2013) The Geology and Mineralogy of the Loulo Mining District, Mali, West Africa: Evidence for Two Distinct Styles of Orogenic Gold Mineralisation. Economic Geology 108:199–227

Lee M, Shin D, Yoo B, Im H, Pak S, Choi S (2019) LA-ICP-MS trace element analysis of arsenopyrite from the Samgwang gold deposit, South Korea, and its genetic implications. Ore Geology Reviews 114:103147

Liu W, Borg SJ, Testemale D, Etschmann B, Hazemann J-L, Brugger J (2011) Speciation and thermodynamic properties for cobalt chloride complexes in hydrothermal fluids at 35–440°C and 600bar: An in-situ XAS study. Geochimica et Cosmochimica Acta 75:1227–1248

Liu W, Migdisov A, Williams-Jones A (2012) The stability of aqueous nickel(II) chloride complexes in hydrothermal solutions: Results of UV–Visible spectroscopic experiments. Geochimica et Cosmochimica Acta 94:276–290

Luukas J, Kousa J, Nironen M, Vuollo J. (2017) Major stratigraphic units in the bedrock of Finland, and an approach to tectonostratigraphic division. In: Nironen M (ed) Bedrock of Finland at the scale 1:1 000 000: Major stratigraphic units, metamorphism and tectonic evolution. Geological Survey of Finland, Espoo, pp 9-40

Mäkelä M (1984) Raahen Laivakankaan kvartsi-arseenikiisu-kultaesiintymä. (in Finnish): The quartz-arsenopyrite-gold mineralisation of Laivakangas, Raahe, Finland. Unpublished M.Sc thesis, University of Turku

Mäkitie H, Lahti S (1991) Seinfijoen kartta-alueen kallioperä. Summary: Pre-Quaternary rocks of the Seinäjoki map-sheet area. Geological Map of Finland 1: 1 000 000. Explanation to the maps of Pre-Quaternary rocks, sheet 2222 Seinäjoki, Espoo

Mäkitie H (1999) Structural analysis and metamorphism of Palaeoproterozoic metapelites in the Seinajoki-Ilmajoki area, western Finland. BULLETIN-GEOLOGICAL SOCIETY OF FINLAND 71:305–328

Mäkitie H (2000) Granitoids (1.89-1.87 Ga), diatexites (1.89-1.88 Ga) and granitic pegmatites (1.80-1.79 Ga), and structural-metamorphic evolution in the Seinäjoki region, western Finland. Ph. D. Thesis

Mäkitie H, Sipilä P, Kujala H, Lindberg A, Kotilainen A (2012) Formation mechanism of the Vaasa Batholith in the Fennoscandian shield: Petrographic and geochemical constraints. Bull Geol Soc Finland 84:141–166

Markl G, Burisch M, Neumann U (2016) Natural fracking and the genesis of five-element veins. Mineral. Deposita 51:703–712

Mathieu L (2019) Detecting magmatic-derived fluids using pyrite chemistry: Example of the Chibougamau area, Abitibi Subprovince, Québec. Ore Geology Reviews 114:103127

Mathieu L, Racicot D (2019) Petrogenetic Study of the Multiphase Chibougamau Pluton: Archaean Magmas Associated with Cu–Au Magmato-Hydrothermal Systems. Minerals 9:174

McCuaig TC, Kerrich R (1998) P—T—t—deformation—fluid characteristics of lode gold deposits: evidence from alteration systematics. Ore Geology Reviews 12:381–453

Mints MV, Glaznev VN, Muravina OM, Sokolova EY (2020) 3D model of Svecofennian Accretionary Orogen and Karelia Craton based on geology, reflection seismics, magnetotellurics and density modelling: Geodynamic speculations. Geoscience Frontiers 11:999–1023

Molnár F, O'Brien H, Lahaye Y, Kurhila M, Middleton A, Johanson B (2017) Multi-stage hydrothermal processes and diverse metal associations in orogenic gold deposits of the Central Lapland greenstone belt, Finland. In: Mercier-Langevin P. et al. (ed) Mineral Resources to Discover, Québec, Canada, pp 63–66

Molnár F, Middleton A, Stein H, O'Brien H, Lahaye Y, Huhma H, Pakkanen L, Johanson B (2018) Repeated syn- and post-orogenic gold mineralisation events between 1.92 and 1.76 Ga along the Kiistala Shear Zone in the Central Lapland Greenstone Belt, northern Finland. Ore Geology Reviews 101:936–959

828 Neumayr P, Cabri LJ, Groves DI, Mikucki EJ, Jackman JA (1993) The mineralogical distribution of gold and relative timing
829 of gold mineralisation in two Archaean settings of high metamorphic grade in Australia. Canadian Mineralogist
830 31:711–725
831 Nironen M (2005) Proterozoic orogenic granitoid rocks. In: Lehtinen M, Nurmi PA, Rämö OT (eds) Precambrian geology
832 of Finland: Key to the evolution of the Fennoscandian shield, 1. ed. Elsevier, Amsterdam, pp 443–480
833 Nironen M, Lahtinen R, Koistinen T. (2002) Subdivision of Finnish bedrock: an attempt to harmonize terminology.
834 Geologi 54 1:8–14
835 Novoselov K, Belogub E, Kotlyarov V, Mikhailov A (2015) Ore mineralogy and formation conditions of the Pirunkoukku
836 gold occurrence (Finland). ejm 27:639–649
837 Ohmoto H (1986) Stable isotope geochemistry of ore deposits. In: Valley JW, Taylor HP, O'Neil JR (eds) Stable Isotopes
838 in High Temperature Geological Processes, Chapter 14. De Gruyter, Berlin, Boston, pp 491–560
839 Oliveira CG de, Oliveira FB de, Della Giustina MES, Marques GC, Dantas EL, Pimentel MM, Buhn BM (2016) The Chapada
840 Cu–Au deposit, Mara Rosa magmatic arc, Central Brazil: Constraints on the metallogenesis of a Neoproterozoic
841 large porphyry-type deposit. Ore Geology Reviews 72:1–21
842 Pankka HS, Vanhanen EJ (1992) Early proterozoic Au-Co-U mineralisation in the Kuusamo district, northeastern
843 Finland. Precambrian Research 58:387–400
844 Patten CGC, Molnár F, Pitcairn IK, Kolb J, Mertanen S, Hector S (2022) Multi-source and multi-stage metal mobilisation
845 during the tectonic evolution of the Central Lapland Greenstone Belt, Finland: implications for the formation of
846 orogenic Au deposits. Mineral. Deposita
847 Patten CGC, Pitcairn IK, Molnár F, Kolb J, Beaudoin G, Guilmette C, Peillod A (2020) Gold mobilisation during
848 metamorphic devolatilisation of Archean and Paleoproterozoic metavolcanic rocks. Geology 48:1110–1114
849 Peltonen P (2005) Svecofennian mafic-ultramafic intrusions. In: Lehtinen M, Nurmi PA, Rämö OT (eds) Precambrian
850 geology of Finland: Key to the evolution of the Fennoscandian shield, 1. ed. Elsevier, Amsterdam, pp 407–442
851 Pilote, P., Robert, F., Sinclair, W.D., Kirkham, R.V., and Daigneault, R. (1995) Porphyry-type mineralisation in the Doré
852 Lake complex: Clark Lake and Merrill Island areas, Day 3: Geological Survey of Canada, Open File Report 3143, p.
853 65–86.
854 Pitcairn IK, Teagle DAH, Craw D, Olivo GR, Kerrich R, Brewer TS (2006) Sources of Metals and Fluids in Orogenic Gold
855 Deposits: Insights from the Otago and Alpine Schists, New Zealand. Economic Geology 101:1525–1546

Pitcairn IK, Leventis N, Beaudoin G, Faure S, Guilmette C, Dubé B (2021) A metasedimentary source of gold in Archean orogenic gold deposits. Geology 49:862–866

Qiu Z-J, Fan H-R, Goldfarb R, Tomkins AG, Yang K-F, Li X-C, Xie L-W, Liu X (2021) Cobalt concentration in a sulfidic sea and mobilisation during orogenesis: Implications for targeting epigenetic sediment-hosted Cu-Co deposits. Geochimica et Cosmochimica Acta 305:1–18

Ridley JR, Diamond LW (2000) Fluid chemistry of orogenic lode gold deposits and implications for genetic models. In: Hagemann SG, Brown PE (eds) Gold in 2000. Society of Economic Geologists, [Littleton, Colorado], pp 141–162

Scharrer M, Kreissl S, Markl G (2019) The mineralogical variability of hydrothermal native element-arsenide (five-element) associations and the role of physicochemical and kinetic factors concerning sulfur and arsenic. Ore Geology Reviews 113:103025

Sharp ZD, Essene EJ, Kelly WC (1985) A re-examination of the arsenopyrite geothermometer: pressure considerations and applications to natural assemblages. Canadian Mineralogist 23:517–534

Sipilä E (1983) Koboltti-kulta-aiheen (M19/2431/-88/1/10) jatkotutkimukset Ylivieskan Kurulassa 1978-83. (in Finnish)

Sipilä E (1988) Kurulan kulta-koboltti-turmaliinibreksian lisäselvitys Winkie-kairauksella 1985. (in Finnish)

Sundblad K, Weihed P, Billström K, Markkula H, Mäkelä M (1993) Source of metals and age constraints for epigenetic gold deposits in the Skellefte and Pohjanmaa districts, central part of the Fennoscandian Shield. Mineralium Deposita 28:181–190

Tapio J, Ranta J-P, Cook N, Lahaye Y, O'Brien H (2021) Paleoproterozoic Rajapalot Au-Co system associated with evaporites: Chemical composition and boron isotope geochemistry of tourmaline, and sulfur isotopes of sulfates, Peräpohja belt, northern Finland. Precambrian Research 365:106410

Tomkins AG, Mavrogenes JA (2001) Redistribution of Gold within Arsenopyrite and Lollingite during Pro- and Retrograde Metamorphism: Application to Timing of Mineralisation. Economic Geology 96:525–534

Vaarma M (1990) Pohjanmaan liuskevyöhykkeen geologia Evijärven alueella. Phil. Lic. Thesis

Vaarma M, Pipping F (1997) Pre-Quaternary rocks of the Alajärvi and Evijärvi map-sheet areas (in Finnish with English summary). Explanation to the maps of Pre-Quaternary rocks. Sheets 2313 and 2314. Geological map of Finland 1: 100 000. Geol. Surv. Finland

Vanhanen E (2001) Geology, mineralogy and geochemistry of the Fe-Co- Au-(U) deposits in the Paleoproterozoic Kuusamo Schist Belt, northeastern Finland. Bulletin, Espoo, Finland

Vanhanen E, Cook NDJ, Hudson MR, Dahlenborg L, Ranta J-P, Havela T, Kinnunen J, Molnár F, Prave AR, Oliver NHS (2015) The Rompas Prospect, Peräpohja Schist Belt, Northern Finland. In: Mineral Deposits of Finland. Elsevier, pp 467–484

Vasilopoulos M, Molnár F, O'Brien H, Lahaye Y, Lefèbvre M, Richard A, André-Mayer A-S, Ranta J-P, Talikka M (2021) Geochemical signatures of mineralizing events in the Juomasuo Au–Co deposit, Kuusamo belt, northeastern Finland. Mineral. Deposita 56:1195–1222

Vasilopoulos M, Molnár F, Ranta J-P, O'Brien H (2022) Mineralogical, lithogeochemical and sulfide trace element characteristics of the Hirvilavanmaa Au-only and the base metal-rich Naakenavaara orogenic gold deposits in the Central Lapland belt, northern Finland. Journal of Geochemical Exploration:107132

Witt WK, Hagemann SG, Roberts M, Davies A (2020) Cobalt enrichment at the Juomasuo and Hangaslampi polymetallic deposits, Kuusamo Schist Belt, Finland: a role for an orogenic gold fluid? In: Miner Deposita, vol. 55, n° 2, p. 381–388.

Yardley BWD, Graham JT (2002) The origins of salinity in metamorphic fluids. Geofluids 2:249–256

Yardley BWD (2005) 100th Anniversary Special Paper: Metal Concentrations in Crustal Fluids and Their Relationship to Ore Formation. Economic Geology 100:613–632

Yund RA, Kullerud G (1966) Thermal Stability of Assemblages in the Cu-Fe-S System. J. Petrology 7:454–488

Zhao H-X, Frimmel HE, Jiang S-Y, Dai B-Z (2011) LA-ICP-MS trace element analysis of pyrite from the Xiaoqinling gold district, China: Implications for ore genesis. Ore Geology Reviews 43:142–153

# 11 HIGHLIGHTS

- Gold enrichment is related to two hydrothermal events: As-Au(-Co-Ni) and Cu(-Au)
- Co-Ni and Cu enrichments are controlled by two independent hydrothermal events
- Cu-enrichment is not related to Cu(-Au) porphyry mineralization
- Intensity of the mineralizing events and redox control the metal content/diversity
- Source rock diversity likely controls the metal content of the ore fluids

909 Table 1



| Laivakangas (wt.%) | n | Fe | δ | Co | δ | Ni | δ | Cu | δ | Ag | δ | Au | δ | Zn | δ | As | δ | Sb | δ | Bi | δ | S | δ | Hg | δ | Total | δ |
|---|---|---|---|---|---|---|---|---|---|---|---|---|---|---|---|---|---|---|---|---|---|---|---|---|---|---|---|
| Arsenopyrite | 111 | 33,318 | 0,785 | 0,323 | 0,425 | 0,174 | 0,295 | <LOD | <LOD | <LOD | <LOD | <LOD | <LOD | <LOD | <LOD | 48,115 | 0,715 | <LOD | <LOD | <LOD | <LOD | 19,108 | 0,582 | <LOD | <LOD | 101,115 | 0,651 |
| Chalcopyrite | 59 | 29,711 | 0,627 | <LOD | <LOD | <LOD | <LOD | 33,867 | 0,686 | 0,024 | 0,015 | <LOD | <LOD | 0,018 | 0,046 | 0,078 | 0,203 | <LOD | <LOD | <LOD | <LOD | 34,635 | 0,399 | <LOD | <LOD | 98,120 | 1,041 |
| Löllingite | 51 | 26,874 | 1,064 | 0,543 | 0,439 | 0,522 | 0,512 | <LOD | <LOD | <LOD | <LOD | <LOD | <LOD | <LOD | <LOD | 69,817 | 1,879 | <LOD | <LOD | 0,383 | 2,412 | 2,185 | 0,425 | <LOD | <LOD | 100,242 | 0,612 |
| Pyrite | 52 | 43,431 | 3,249 | 0,135 | 0,338 | 0,042 | 0,084 | 0,861 | 1,071 | 0,032 | 0,031 | <LOD | <LOD | 0,018 | 0,037 | 2,389 | 3,208 | <LOD | <LOD | 0,121 | 0,294 | 49,804 | 4,179 | <LOD | <LOD | 98,413 | 1,325 |
| Pyrrhotite | 20 | 59,545 | 0,257 | <LOD | <LOD | <LOD | <LOD | 0,050 | 0,033 | <LOD | <LOD | <LOD | <LOD | <LOD | <LOD | 0,054 | 0,122 | <LOD | <LOD | <LOD | <LOD | 38,955 | 0,527 | <LOD | <LOD | 98,593 | 0,415 |

| Jouhineva (wt.%) | n | Fe | δ | Co | δ | Ni | δ | Cu | δ | Ag | δ | Au | δ | Zn | δ | As | δ | Sb | δ | Bi | δ | S | δ | Hg | δ | Total | δ |
|---|---|---|---|---|---|---|---|---|---|---|---|---|---|---|---|---|---|---|---|---|---|---|---|---|---|---|---|
| Arsenopyrite | 113 | 32,528 | 2,078 | 1,531 | 1,745 | 0,095 | 0,118 | <LOD | <LOD | <LOD | <LOD | <LOD | <LOD | <LOD | <LOD | 47,646 | 1,351 | 0,032 | 0,025 | 0,051 | 0,041 | 19,587 | 1,105 | <LOD | <LOD | 101,507 | 0,513 |
| Bornite | 5 | 10,960 | 0,129 | <LOD | <LOD | <LOD | <LOD | 61,730 | 1,396 | 0,045 | 0,007 | <LOD | <LOD | <LOD | <LOD | 0,027 | 0,023 | <LOD | <LOD | 0,045 | 0,041 | 25,860 | 0,356 | <LOD | <LOD | 98,687 | 1,851 |
| Chalcopyrite | 28 | 29,247 | 3,116 | <LOD | <LOD | 0,008 | 0,022 | 33,847 | 0,471 | 0,026 | 0,029 | <LOD | <LOD | 0,156 | 0,789 | 0,668 | 2,633 | 0,034 | 0,101 | 0,043 | 0,043 | 34,635 | 1,120 | <LOD | <LOD | 98,667 | 1,563 |
| Cubanite | 2 | 36,060 | 0,170 | <LOD | <LOD | 0,193 | 0,044 | 17,360 | 1,216 | 0,126 | 0,018 | <LOD | <LOD | 0,011 | 0,009 | 0,700 | 0,344 | <LOD | <LOD | 0,074 | 0,076 | 42,595 | 0,106 | <LOD | <LOD | 97,166 | 0,416 |
| Digenite | 4 | 0,024 | 0,014 | <LOD | <LOD | <LOD | <LOD | 78,038 | 0,331 | 0,061 | 0,020 | <LOD | <LOD | <LOD | <LOD | <LOD | <LOD | <LOD | <LOD | 0,044 | 0,029 | 21,123 | 0,314 | 0,038 | 0,016 | 99,335 | 0,241 |
| Pyrite | 22 | 45,157 | 2,005 | 0,008 | 0,015 | 0,104 | 0,075 | 1,359 | 3,390 | 0,021 | 0,037 | <LOD | <LOD | <LOD | <LOD | 0,489 | 0,834 | <LOD | <LOD | <LOD | <LOD | 51,409 | 2,064 | <LOD | <LOD | 98,602 | 0,953 |
| Tennantite | 14 | 10,172 | 6,849 | 0,015 | 0,016 | 0,069 | 0,092 | 37,191 | 6,375 | 0,080 | 0,066 | <LOD | <LOD | 2,676 | 0,790 | 17,098 | 4,356 | 0,042 | 0,049 | <LOD | <LOD | 31,376 | 3,420 | <LOD | <LOD | 98,744 | 0,955 |

| Huhta (wt.%) | n | Fe | δ | Co | δ | Ni | δ | Cu | δ | Ag | δ | Au | δ | Zn | δ | As | δ | Sb | δ | Bi | δ | S | δ | Hg | δ | Total | δ |
|---|---|---|---|---|---|---|---|---|---|---|---|---|---|---|---|---|---|---|---|---|---|---|---|---|---|---|---|
| Arsenopyrite | 50 | 34,223 | 0,687 | <LOD | <LOD | 0,029 | 0,063 | <LOD | <LOD | <LOD | <LOD | <LOD | <LOD | <LOD | <LOD | 46,750 | 1,777 | 0,036 | 0,039 | <LOD | <LOD | 20,168 | 1,347 | <LOD | <LOD | 101,335 | 0,826 |
| Chalcopyrite | 24 | 30,047 | 0,720 | <LOD | <LOD | <LOD | <LOD | 32,041 | 1,716 | 0,019 | 0,010 | <LOD | <LOD | <LOD | <LOD | 1,931 | 2,139 | <LOD | <LOD | <LOD | <LOD | 34,801 | 1,008 | <LOD | <LOD | 98,892 | 1,316 |
| Pyrrhotite | 17 | 58,945 | 2,586 | <LOD | <LOD | <LOD | <LOD | <LOD | <LOD | <LOD | <LOD | <LOD | <LOD | <LOD | <LOD | 2,323 | 4,638 | <LOD | <LOD | <LOD | <LOD | 37,622 | 2,401 | <LOD | <LOD | 98,974 | 0,900 |
| Pyrite | 29 | 45,908 | 0,838 | <LOD | <LOD | <LOD | <LOD | <LOD | <LOD | <LOD | <LOD | <LOD | <LOD | <LOD | <LOD | 0,368 | 0,632 | <LOD | <LOD | <LOD | <LOD | 51,852 | 1,273 | <LOD | <LOD | 98,213 | 1,920 |

| Kurula (wt.%) | n | Fe | δ | Co | δ | Ni | δ | Cu | δ | Ag | δ | Au | δ | Zn | δ | As | δ | Sb | δ | Bi | δ | S | δ | Hg | δ | Total | δ |
|---|---|---|---|---|---|---|---|---|---|---|---|---|---|---|---|---|---|---|---|---|---|---|---|---|---|---|---|
| Arsenopyrite | 78 | 30,212 | 1,828 | 3,233 | 1,590 | 0,167 | 0,157 | <LOD | <LOD | <LOD | <LOD | <LOD | <LOD | <LOD | <LOD | 49,414 | 1,716 | <LOD | <LOD | 0,091 | 0,393 | 18,112 | 1,151 | <LOD | <LOD | 101,368 | 0,598 |
| Chalcopyrite | 10 | 29,992 | 0,178 | <LOD | <LOD | <LOD | <LOD | 33,614 | 0,813 | 0,022 | 0,011 | <LOD | <LOD | 0,059 | 0,094 | 0,041 | 0,028 | <LOD | <LOD | <LOD | <LOD | 34,927 | 0,287 | <LOD | <LOD | 98,700 | 0,640 |
| Löllingite | 4 | 26,505 | 0,238 | 0,705 | 0,077 | 0,546 | 0,045 | <LOD | <LOD | <LOD | <LOD | <LOD | <LOD | <LOD | <LOD | 69,065 | 0,474 | <LOD | <LOD | <LOD | <LOD | 2,308 | 0,450 | <LOD | <LOD | 99,213 | 0,479 |
| Pyrrhotite | 5 | 60,170 | 0,050 | <LOD | <LOD | 0,010 | 0,007 | <LOD | <LOD | <LOD | <LOD | <LOD | <LOD | <LOD | <LOD | 0,042 | 0,018 | <LOD | <LOD | <LOD | <LOD | 38,634 | 0,405 | <LOD | <LOD | 98,956 | 0,428 |
| Pyrite | 10 | 46,120 | 0,351 | <LOD | <LOD | 0,026 | 0,025 | 0,396 | 0,576 | <LOD | <LOD | <LOD | <LOD | <LOD | <LOD | 0,531 | 0,638 | <LOD | <LOD | <LOD | <LOD | 52,413 | 0,716 | <LOD | <LOD | 99,498 | 0,869 |
| Rammelsbergite | 1 | 7,890 | - | 0,108 | - | 25,810 | - | <LOD | - | <LOD | - | <LOD | - | <LOD | - | 59,910 | - | 0,053 | - | <LOD | - | 2,850 | - | <LOD | - | 96,742 | - |
| Safflorite | 21 | 20,967 | 2,853 | 6,111 | 1,886 | 0,969 | 0,546 | <LOD | <LOD | <LOD | <LOD | <LOD | <LOD | <LOD | <LOD | 71,046 | 1,167 | <LOD | <LOD | 0,087 | 0,088 | 1,420 | 0,671 | <LOD | <LOD | 100,645 | 0,480 |
| Skutterudite | 13 | 2,755 | 0,998 | 16,286 | 2,005 | 2,025 | 0,819 | <LOD | <LOD | <LOD | <LOD | <LOD | <LOD | <LOD | <LOD | 78,814 | 0,664 | <LOD | <LOD | <LOD | <LOD | 0,202 | 0,077 | <LOD | <LOD | 100,169 | 0,768 |

910

| | Fe | Co | Ni | Cu | Ag | Au | Zn | As | Sb | Bi | S | Hg |
|---|---|---|---|---|---|---|---|---|---|---|---|---|
| Det. limit Laivakangas (ppm) | 71 | 81 | 70 | 718 | 102 | 202 | 95 | 211 | 249 | 428 | 95 | 337 |
| Det. limit Jouhineva(ppm) | 70 | 80 | 70 | 743 | 102 | 200 | 94 | 213 | 245 | 416 | 94 | 329 |
| Det. limit Huhta (ppm) | 69 | 81 | 68 | 731 | 99 | 197 | 92 | 204 | 243 | 410 | 96 | 323 |
| Det. limit Kurula (ppm) | 104 | 101 | 111 | 1295 | 135 | 329 | 148 | 336 | 363 | 695 | 153 | 543 |

912 Tabl

913

| Deposit | Mineral | n | mean $\delta^{34}S$ (‰) | 2σ (‰) | Min. value | Max. value |
|---|---|---|---|---|---|---|
| Laivakangas | Apy | 12 | +1.95 | 0.56 | +1.52 | +2.43 |
| Laivakangas | Po | 3 | +2.55 | 0.13 | +2.47 | +2.63 |
| Laivakangas | Py | 3 | +2.37 | 0.04 | +2.34 | +2.39 |
| Laivakangas | Ccp | 9 | +2.77 | 0.99 | +2.04 | +3.17 |
| Jouhineva | Apy | 11 | +7.71 | 0.77 | +7.20 | +8.21 |
| Jouhineva | Ccp | 9 | +6.03 | 0.17 | +5.87 | +6.17 |
| Huhta | Po | 6 | +5.12 | 0.08 | +5.04 | +5.18 |
| Huhta | Apy | 12 | +5.67 | 1.31 | +4.44 | +6.55 |
| Kurula | Ccp | 3 | +1.43 | 0.07 | +1.39 | +1.47 |
| Kurula | Apy | 12 | +3.02 | 0.20 | +2.83 | +3.17 |
| Kurula | Po | 6 | +2.48 | 0.33 | +2.19 | +2.67 |